# On Atmospheric Waves

*By* A. WIIN-NIELSEN

The Collstrop Foundation


Matematisk-fysiske Meddelelser **48**

Det Kongelige Danske Videnskabernes Selskab
*The Royal Danish Academy of Sciences and Letters*

Commission Agent: C. A. Reitzels Forlag
Copenhagen 2001

## Abstract

A major purpose of the paper is to discuss the various wave types (inertial waves, thermal waves, Rossby waves) that appear in the baroclinic atmosphere. The interaction between these wave types will also be treated, and the relations between the calculated waves and the observed waves will be discussed. For simplicity and clarity the wave types will also be discussed one by one.

A second purpose is to discuss the general structure of the most important weather-related waves. This will be done by using a greatly simplified model including for some purposes both external heating and dissipation of the kinetic energy leading to a general description of the structure of the model waves.

An expanded study of inertial motion will be handled using the spherical equations, and the thermal wave will be discussed in details using a vertical model of these waves which does not depend on the horizontal scale.



Printed in Denmark by Special-Trykkeriet Viborg a-s
ISSN 0023-3323. ISBN 87-7876-268-5

# 1. Introduction

The atmosphere contains a variety of phenomena. Some of these are of a local nature such as the land and sea breeze that may be described in a simple way by considering the changes in the daily variations of the heating over land and over water. Other types are of a global kind appearing everywhere in the atmosphere although differences may be observed depending on the latitude and the distribution of continents and oceans. The analyses of the global atmosphere at many vertical levels, made possible due to expansions of the network of meteorological observations supplemented by information from special Earth-observing satellites, indicate that the motion of the atmosphere in middle latitudes has a wave-like character. The wavelength may vary greatly from very long waves with a maximum wavelength equal to the length of the latitude circle to shorter waves with a wavelength of, say, 1000 km. The very long waves appear to consist of a stationary part and a moving part. The stationary part is related to the differences in atmospheric behavior over the continents and over the oceans (Smagorinsky, 1953) and to the existence of major mountain ranges such as the Rocky Mountains in North America and the Himalayas in Asia (Charney and Eliassen, 1949). The transient waves which will be included in the present study may be long or short waves. The analyses of the observed kinetic energy as a function of the wavelength (Wiin-Nielsen, 1967, 1999 and 2000) show that the maximum kinetic energy of the transient waves is found for wavelengths between 4000 and 7000 km corresponding in the middle latitudes to wave numbers 7 and 4.

These facts may to some extent be explained by the theories of the stability of the zonal flow when this flow is disturbed by small disturbances. Such investigations were initiated by Charney (1947), and numerous studies of this kind, too many to list all of them, have been carried out since then.

The atmosphere is analysed from observations twice a day, normally at 0 and 12 UTC. The analyses are presented using surfaces in which the pressure is constant. Operationally, such analyses are made at the pressure surfaces 1000, 850, 700, 500, 300, 200 and 100 hPa, but analyses at even lower pressure levels may be included. For each pressure surface we find analyses of the geopotential (g*z, where g is the

(constant) gravity), the temperature, the humidity and the two components of the horizontal wind.

In middle and high latitudes it is observed that the horizontal wind has a strong tendency to be directed as a tangent to the isolines for the geopotential. If this relation was exact, the atmospheric horizontal wind would be called a *geostrophic wind* which is defined as the wind that will exist if the horizontal pressure force is balanced by the Coriolis force. Since the pressure force is perpendicular to isolines for the geopotential, and since the Coriolis force in the northern hemisphere points to the right of the horizontal wind, it follows that the *geostrophic wind* will blow along the isolines for the geopotential. The described tendency is not exact. We talk therefore about the *quasi-geostrophic* state of the atmosphere in the middle latitudes.

The first numerical predictions were carried out in 1949-50 (Charney et al., 1950). The model was the most simple one level model assuming horizontal geostrophic flow at 500 hPa. The integration of the model equations took many hours on one of the first 'electronic computers' as they were called at the time. During the following two decades a number of more advanced models were developed. These models were based on the quasi-geostrophic concept. The number of levels in the vertical direction was mostly restricted to two or three levels, but operational models with many more levels have been used later in the development of numerical weather prediction. The quasi-geostrophic models predicted only one parameter, the geopotential, which is proportional to the height of the isobaric surfaces relative to the surface of the Earth. However, the multilevel models permit a calculation of the mean temperature of the layers and the vertical velocity at selected levels. Later models have predicted the total collection of atmospheric parameters, i.e. the three components of the three-dimensional atmospheric wind, the pressure, the temperature, the density and the humidity. Models of this kind are based on the so-called *primitve* equations. During the first decade or so no heating and no dissipation were used in the prediction models, but some models had a term measuring the effect of the large-scale mountains on the atmospheric flow.

Parallel with these developments, models of a different kind were developed. The purpose was to simulate the major aspects of the atmospheric state as an average of the integrations of the model over many days. These models, which later were called '*climate models*', did not make predictions for individual days, but the purpose was to simulate the averaged state of the atmosphere. The verification was therefore a comparison of the model climate with the real climate. The first experiment of this kind was carried out by Phillips (1956) based on a two-level, quasi-geostrophic model with a prescribed forcing in the meridional direction resulting in heating in the low latitudes and cooling in the high latitudes. The heating was linear with respect to the south-north direction and at each point constant during the

whole integration. No heating was prescribed in the west-east direction. After an integration using only the zonal equations, a state of zonal winds and temperatures were developed. Superimposing small, random perturbations in each gridpoint the integrations were continued using now the full equations. The output was a development of moving atmospheric waves. The result was in schematic agreement with the atmospheric wave behavior. Another two-level model based on the primitive equations was developed by Smagorinsky (1963). This model represents the first serious attempt to use the general equations. The experiment started from a state of rest. The results could be described as those by Phillips (1956), but the numerical experiment showed that also the primitive equations could be integrated over many days.

After these pioneering experiments, the models for the numerical weather predictions and for the simulations of the climate have gradually become very similar to each other with respect both to the use of the full equations and the incorporation of both simulated heating and frictional dissipation in the model atmosphere. No significant differences exist between the two kinds of models, but the applications of the models are still quite different. One kind is used to make the best possible weather predictions for the coming few days, while the other kind is used for simulations of the present climate and simulations of possible changes in the climate. While this summary of the developments of atmospheric models for half a century is quite schematic, it should be sufficient to serve as a background for the discussion of the various types of waves which are incorporated in the most general models.

The purpose of the paper is to investigate the creation and the development of the atmospheric waves in middle latitudes. The latitude of 45 degrees north will be used in all calculations. To keep the theoretical considerations at a simple level the space dimensions will be the west-east direction and pressure in the vertical direction. This does not mean that the variations in the south-north direction are unimportant, and these variations will be used in some of the model experiments to verify the results of the simpler model which is treated analytically.

## 2. Wave types

In this section we will consider the various wave types which may be obtained from simplified cases of the atmospheric equations. The speed of the particular wave will be determined, and it will be discussed if such waves have been observed in the atmosphere. If this is the case, the question is: Do these waves influence the weather? By combining the applied simplified equations we may construct less simplified models containing several types of waves. The general equations will

naturally contain all the wave types, and as long as we stay with a set of linear equations we may recognize all the wave types. It should furthermore be possible to investigate whether or not the models will arrive in a state of quasi-geostrophic balance as is observed in the real atmosphere. This is to be expected due to recent studies of the geostrophic adjustment problem (Wiin-Nielsen, 2000). As the most general, but still simple, model for long term integrations we apply a low order spectral model developed recently by Marcussen and Wiin-Nielsen (1999). The zonal flow is described by two trigonometric functions, while the eddies have twice as many components to permit moving waves. The total number of components is 12, and this is the minimal number of components in a model if we want to describe both the eddy transports of sensible heat and of momentum.

## 2a. Inertial waves

As a first example we shall consider the inertial waves which are the waves that will exist if the only force is the Coriolis force. Disregarding any basic motion the governing equations are given in (2.1).

$$\frac{\delta u}{\delta t} = f_o v$$
$$\frac{\delta v}{\delta t} = -f_o u \tag{2.1}$$

In these equations u and v are the horizontal wind components and $f_o$ the Coriolis parameter at a given latitude.

As usual we shall consider perturbations of the type given in (2.2).

$$b = b_a e^{ik(x-ct)} \tag{2.2}$$

In this equation for the perturbations b is an arbitrary scalar variable and $b_a$ the amplitude, while k is the wave number and c the phase velocity. By introducing (2.2) in (2.1) we obtain the phase speed for the inertial waves as given in (2.3).

$$c_I = \pm \frac{f_o}{k};\ k = \frac{2\pi}{L} \tag{2.3}$$

where L is the wavelength. The phase velocity being proportional to the wavelength can be very large for the long waves. If L = 28000 km and the latitude is 45

degrees, the magnitude of the wave speed is about 446 m per s. On the other hand, for L=1000 km we find the positive wave speed to be $c_I$ =15.9 m per s. To find pure inertial waves in the atmosphere is very difficult since they require a vanishing pressure gradient. However, inertial waves have been observed in a few cases where the pressure gradient is small. The influence of the inertial waves will therefore in general be in combination with other wave types.

Only the most simple case using a constant value of the Coriolis' parameter ($f_o$) is treated above. The more detailed analysis of inertial waves using spherical geometry is found in Section 6 of the present paper.

## 2b. Thermal waves

This wave type is obtained when we disregard the Coriolis force, but maintain the pressure force in the equation of motion. In addition, we need the thermal equation and the continuity equation to close the system. Considered in one dimensional space we get the equations as listed in (2.4).

$$\begin{aligned} \frac{\delta u}{\delta t} + \frac{\delta \Phi}{\delta x} &= 0 \\ \frac{\delta}{\delta t}\left(\frac{\delta \Phi}{\delta p}\right) + \sigma\omega &= 0 \\ \frac{\delta u}{\delta x} + \frac{\delta \omega}{\delta p} &= 0 \end{aligned} \qquad (2.4)$$

To avoid too much mathematics for our purpose it is convenient to solve the equations by employing a two-level model. We apply the equation of motion and the continuity equation at 250 and 750 hPa, while the thermodynamic equation is applied at 500 hPa. Adding and subtracting the dynamic equations in the usual way we find that only the thermal terms give non-vanishing contributions. After a little algebra we find the set of equations listed in (2.5).

$$\begin{aligned} \frac{\delta u_T}{\delta t} + \frac{\delta \Phi_T}{\delta x} &= 0 \\ \frac{\delta \Phi_T}{\delta t} - \frac{\sigma P}{2}\omega &= 0 \\ \frac{\delta u_T}{\delta x} + \frac{\omega}{P} &= 0 \end{aligned} \qquad (2.5)$$

In these equations P is half the standard value of the surface pressure ($p_o = 10^5$ Pascal). The system (2.5) is a closed system with three dependent variables. Introducing the wave form given in (2.2) we find after evaluation of the determinant that the speed of the thermal waves is as given in (2.6).

$$c_T = \pm \left(\frac{\sigma P^2}{2}\right)^{1/2} \tag{2.6}$$

We notice that the thermal wave speed is independent of the wavelength. Using a standard value of $\sigma$ we find that the thermal wave speed is about 190 m per s. It appears that the thermal waves in a pure form are not observed in the atmosphere.

A more general investigation of thermal waves is carried out in Section 7 of the present paper.

## 2c. Mixed inertial and thermal waves

It is also easy to formulate a system which contains waves of the two types treated in *2a* and *2b*. The basic equations for such a system are given in (2.7).

$$\begin{aligned} &\frac{\delta u}{\delta t} + \frac{\delta \Phi}{\delta x} - f_o v = 0 \\ &\frac{\delta v}{\delta t} + f_o u = 0 \\ &\frac{\delta}{\delta t}\left(\frac{\delta \Phi}{\delta p}\right) + \sigma\omega = 0 \\ &\frac{\delta u}{\delta x} + \frac{\delta \omega}{\delta p} = 0 \end{aligned} \tag{2.7}$$

We shall also in this case use a two level model for the determination of the wave speeds. As in the previous case we apply the technique of adding and subtracting the equations valid at 250 and 750 hPa. The equation for the 500 hPa level has only the trivial wave speed c = 0, while the determinant for the thermal variable leads to a cubic equation with the roots c = 0 and the two phase speeds listed in (2.8).

$$c = \pm (c_I^2 + c_T^2)^{1/2} \tag{2.8}$$

## 2d. Rossby waves

The Rossby waves with wavelengths of a few thousand kilometers are observed in the atmosphere. They appear as solutions of the barotropic vorticity equation shown in (2.9).

$$\frac{\delta\zeta}{\delta t} + \beta \frac{\delta\psi}{\delta x} = 0 \tag{2.9}$$

The well known solution of this equation using the same expression for the perturbation is shown in (2.10).

$$C_R = -\frac{\beta}{k^2} \tag{2.10}$$

Just as the inertial waves, the Rossby waves give very large negative values for large values of the wavelength. The Rossby waves are observed in the atmosphere, particularly for smaller values of the wavelength, while Rossby waves with the large negative speeds for long waves are unobserved.

## 2e. The general case

The two level model will be used in the general case. To include the beta-effect we need to use the vorticity equation, the divergence equation and the continuity equation at the levels 250 and 750 hPa, while the thermodynamic equation will be applied at the middle level, 500 hPa. After the addition and subtractions of the equations applied at 250 and 750 hPa we obtain the equations valid at 500 hPa and for the layer between 250 and 750 hPa. The equations contain no advection terms and are linear. The equations applicable at 500 hPa are with no basic current trivial and permit only $c = -c_R$. The equations for the thermal parameters are given in (2.11).

$$\begin{aligned} ik\,(c + c_R)\,\psi_T - f_o\chi_T &= 0 \\ f_o\psi_T + ik\,(c + c_R)\,\chi_T - \Phi_T &= 0 \\ -ikc\Phi_T - \frac{\sigma P}{2}\omega &= 0 \\ -k^2\chi_T + \frac{1}{P}\omega &= 0 \end{aligned} \tag{2.11}$$

Evaluating the determinant for the system (2.11) and setting it equal to zero we find equation (2.12) for the phase speeds.

$$(c + c_R)^3 - c_R (c + c_R)^2 - (c_I^2 + c_T^2)(c + c_R) + c_I^2 c_R = 0 \qquad (2.12)$$

It is seen that (2.12), which is the most general equation for the system under consideration, contains the three wave velocities found in the simple cases investigated in the previous subsections. The equations valid in the subsections can as a matter of fact be obtained by setting one or two of the three velocities $c_R$, $c_T$ and $c_I$ equal to zero. Equation (2.12), being of the third degree, could be solved in a closed form, but since the interest is in solutions as a function of the wavelength, it is more convenient to obtain the solutions by applying a root-finding numerical program. From the equation itself it can be shown that only real roots are present, since the determinant is negative for all wavelengths. This statement is confirmed by the numerical determination which also provides the imaginary part of the root. They are zero in all cases.

The three solutions of (2.12) are two wave velocities, one positve and the other

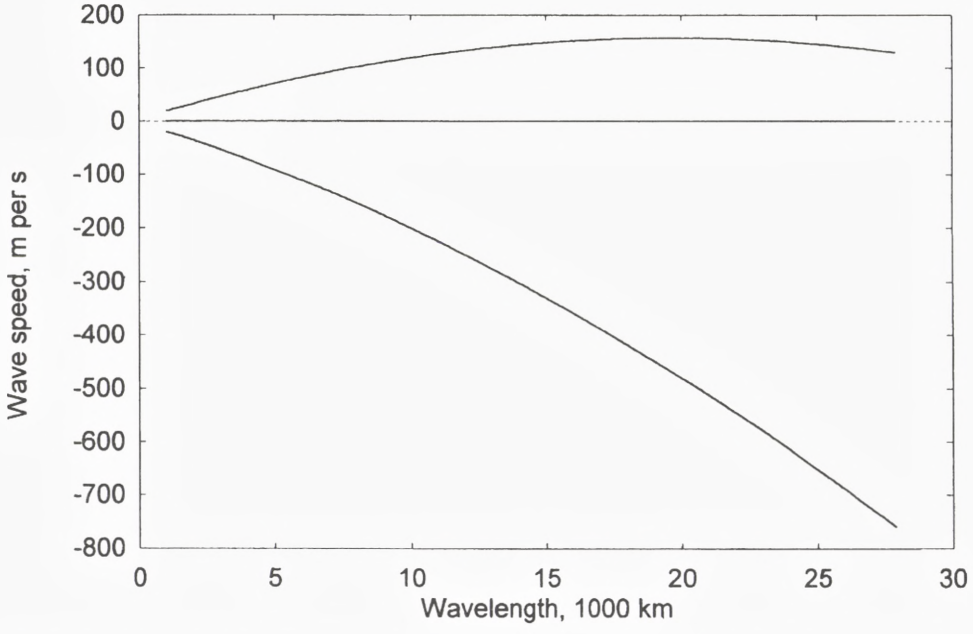


Fig. 1: Wave speeds for the three waves, two fast waves moving in opposite directions and a slow wave.

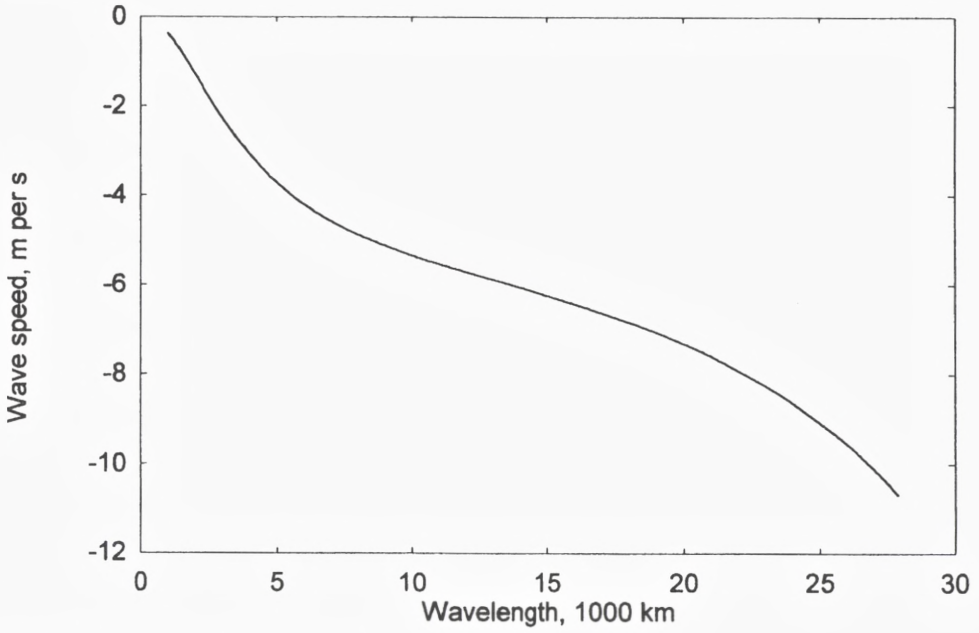


Fig. 2: Wave speed for the slow wave for n = 1.

negative, with numerically large values for all wavelengths and one velocity with moderate values for all wavelengths. Figure 1 shows all three wave speeds as a function of wavelength, while Figure 2 shows the slowly moving wave component. From observational studies of the velocities of long transient waves it is evident that they move with speeds much smaller than those displayed in Figure 1. For comparative reasons we may consider the wave velocities in special cases. One may naturally consider special cases with $c_I = 0$ or $c_T = 0$, but no new information is obtained from these special cases.

It is these facts that created the desire to construct the so-called quasi-geostrophic or quasi-nondivergent models that dominated the operational numerical forecasting in the 1950s and 1960s. However, the Rossby type of wave solutions should not be filtered out, and we therefore still have a problem with respect to the velocity of the very long waves. It should be recalled that observational studies of very long waves show that these waves are partly stationary waves created by mountains and planetary heat sources and partly retrograde transient waves with velocities smaller than the Rossby velocity.

One reason for the very large velocities found in this study could be the neglect of the meridional scale, the missing mountain and heating effects and the simple

lower boundary condition. While the condition that the vertical p-velocity vanishes at the top of the atmosphere is correct, it is doubtful if the same condition at the bottom of the atmosphere is sufficiently accurate. At 1000 hPa we may more correctly say that the vertical p-velocity may be written in the form shown in equation (2.13).

$$\omega_s \approx \frac{\delta p}{\delta t} \approx \frac{\delta p}{\delta z} \frac{\delta z}{\delta t} \tag{2.13}$$

Using the hydrostatic equation and replacing the height by the streamfunction we find the expression given in (2.14). This expression, valid at the 1000 hPa surface, has to be related to the streamfunction at 500 hPa in a barotropic model.

$$\frac{f_o}{p_o} \omega_o \approx \frac{f_o^2}{RT_o} \left(\frac{\delta \psi}{\delta t}\right)_o \tag{2.14}$$

A term as estimated in (2.14) was added to the barotropic vorticity equation in the early days of numerical weather prediction with the purpose of making the wave speed of the very long waves numerically smaller. The coefficient in the term is estimated in (2.15).

$$C_s = \frac{f_o^2}{RT_o} \approx 0.1 x 10^{-12} m^{-2} \tag{2.15}$$

With the above value we get a reduction of the wave speed for the very long waves (L= 28000 km) from -314 to about -105 m per s. The latter value is still much larger than the observed retrogression of the very long waves. However, in numerical forecasting in the 1950's and 1960's, a term of this kind was added to the barotropic vorticity equation, but the coefficient $C_s$ was not given the value estimated above, but determined empirically by making a number of forecasts using various values of the coefficient and selecting the one that on average gave the smallest errors in the forecast. The selected value is larger than the estimate given in (2.15) as seen from Cressman (1958) and Wiin-Nielsen (1959). The procedure described above may naturally also be incorporated in baroclinic models. We shall in the following consider the standard two-level model changed in such a way that the lower boundary condition ($\omega = 0$) is replaced by a more realistic condition.

We start from the relation given in (2.14). The streamfunction at 1000 hPa is replaced by the expression given in (2.16).

$$\psi_o = \psi_* - 2\psi_T \tag{2.16}$$

In the vorticity equation at level 3 (750 hPa) we have to add a term on the right hand side as given in (2.17).

$$\frac{f_o}{2P}\,\omega_4 \approx -\frac{f_o^2}{RT_s}\,\frac{\delta(\psi_* - 2\psi_T)}{\delta t} \tag{2.17}$$

A determination of the real and complex wave speed is carried out for the model with the nonzero vertical p-velocity at the lower boundary. From the evaluation it is seen that for this model we also get for the very long waves a reduction of the wave speed to a little more than –100 m per s which is almost the same as in the one-level model considered above.

This section of the paper has presented the various types of waves which have been discussed in very simple atmospheric models having no zonal motion. The question of the importance of the lower boundary condition on ω has been determined with the classical two-level quasi-nondivergent model. A basic zonal motion with horizontal and/or vertical variations are necessary to discuss atmospheric instabilities. Additional problems of this type will be discussed in other parts of the paper.

## 3. Baroclinic instabilities

To investigate the baroclinic instabilities that may be present in the models we shall add the advective terms in the equations. This can be done while we at the same time limit the wave specification to have a dependence on the west-east coordinate (x) and time (t). One possibility would be to select the standard two level model as was done in Section 2, where vorticities and divergencies are used at an upper level (250 hPa) and a lower level (750 hPa), while the thermodynamic equation is applied at the middle level (500 hPa). When this model is used, we have only one temperature level in the model, and any measure of the vertical variation of the temperature can only be included as a standard value. The vertical p-velocity is present at 500 hPa only.

A second possibility may be considered. In a two-level model formulated originally by Gates (1961) the thermodynamic equation is applied at the upper (250 hPa) and the lower (750 hPa) levels giving two temperatures in each vertical column. In such a model we also need the vertical velocities at these two levels. It is assumed that both of them are a fraction (say $^1/_2$) of the vertical velocity at 500 hPa level. Gates (1961) assumed further in his analysis of baroclinic stability that

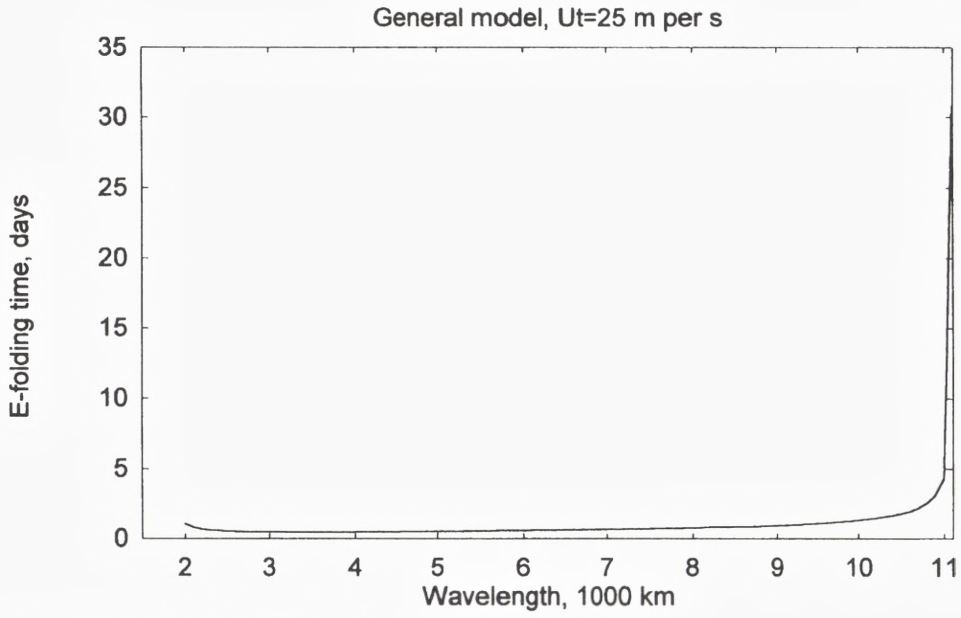


Fig. 3: The general model: Stability analysis for medium-range waves.

the static stability is constant. However, this simplification was not introduced in the model for the baroclinic stability analysis by the author (Wiin-Nielsen, 1962). We shall therefore be able to analyse both models and determine the difference in the stabilities of the two models. To distinguish between the two models we shall name the first model the 'general model', while the model with a constant static stability will be called the balanced model. The detailed perturbation equations may be found in the paper by Wiin-Nielsen (1962).

The results of the baroclinic stability analysis for the general model may be found in Figure 3 for the medium-range waves assuming that the vertical windshear in the basic state is 25 m per s. The same value will be used in all the comparisons in the present section. Instability is found for wavelengths between about 2000 km and 11000 km with an e-folding time as short as half a day due to the rather large value of $U_T$. Figure 4 shows the wave speeds for the same model. We notice that the large negative values of the wave speed for long waves (the beta-effect) are present. Turning to the very long waves we see from Figure 5 that also the long waves are unstable with e-folding times which are larger than for the short waves. All e-folding times are in fact larger than two days.

Figure 6 gives the e-folding time for the balanced model. We notice that the smallest e-folding time are still of the order of half a day. In addition, the instability

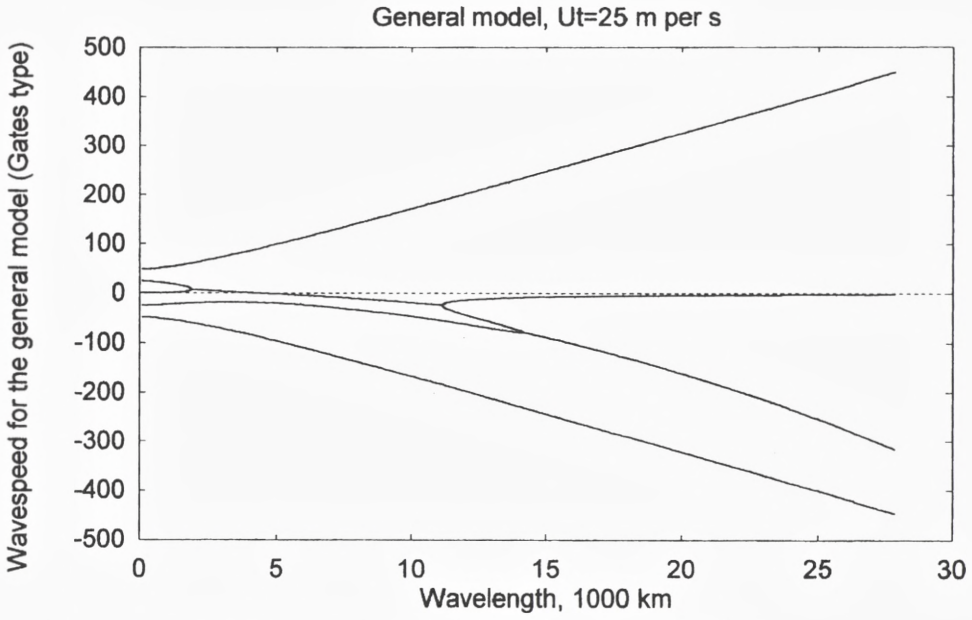


Fig.4: The general model: Wave speeds, m per s as a function of the wavelength.

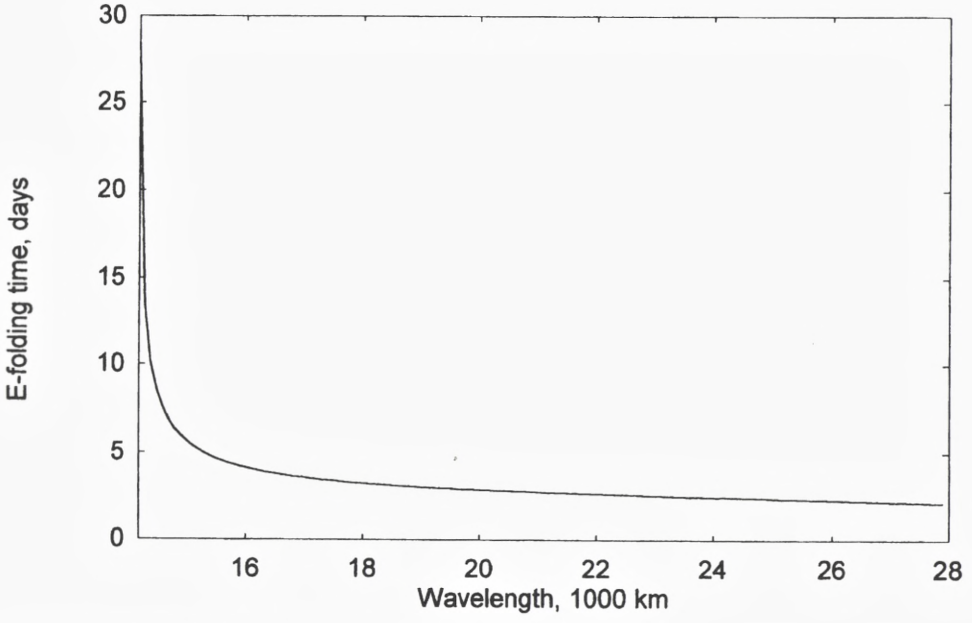


Fig. 5: The general model: Stability analysis for the very long waves.

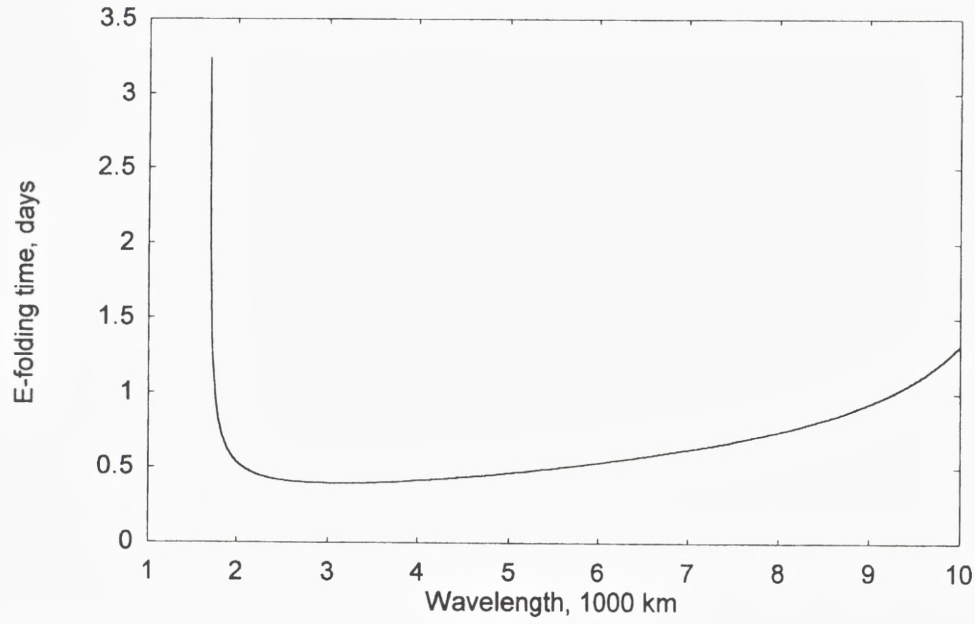


Fig. 6: The balanced model: E-folding times in days.

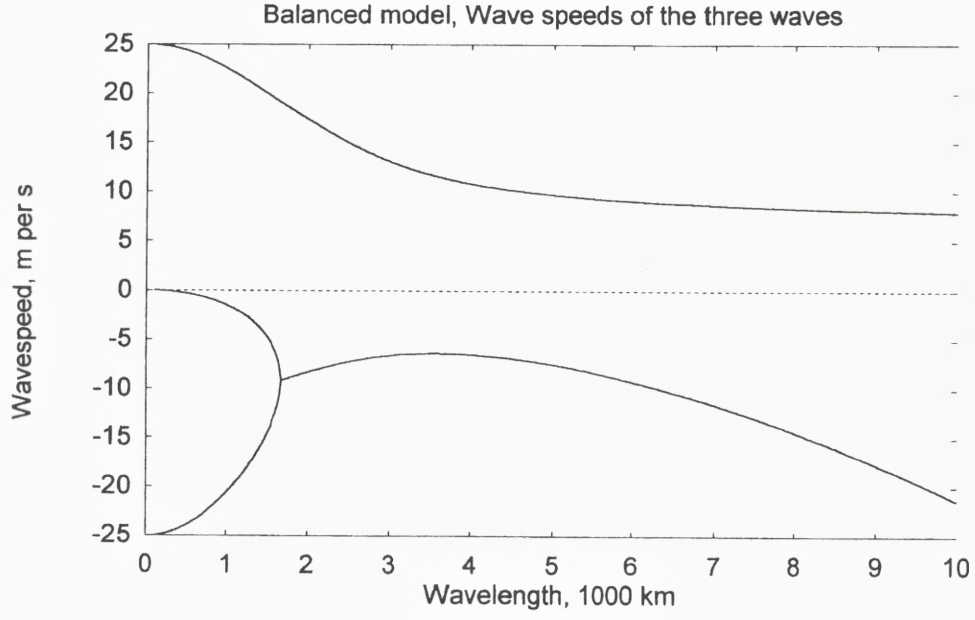


Fig. 7: Waves speeds, m per s, for the three waves in the model.

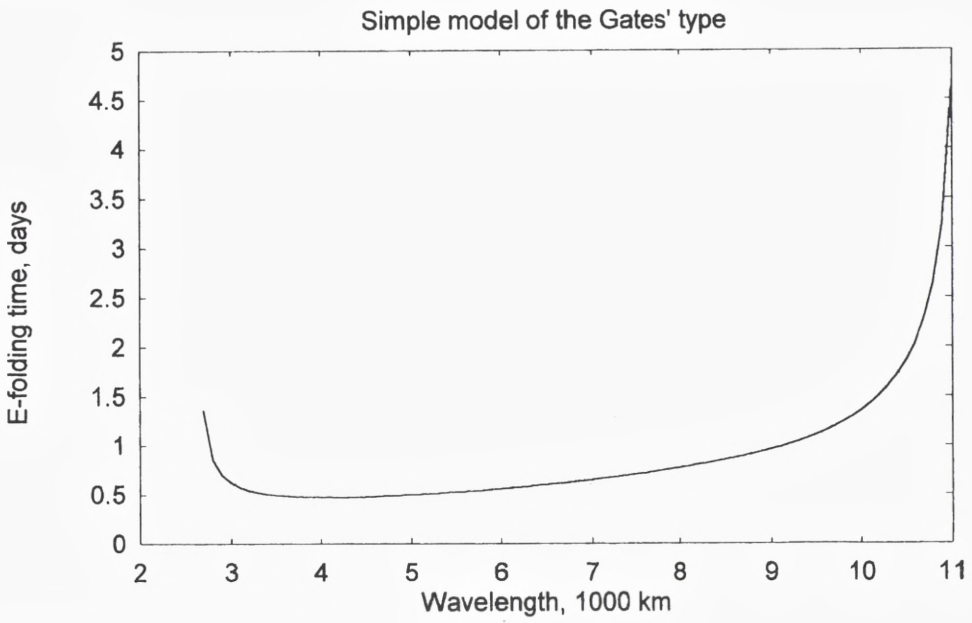


Fig. 8: E-folding times, days, for $U_T$ = 25 m per s.

starts at slightly smaller values of the wavelength. Another important point is that no instabilities are found for the very long waves. Figure 7 shows the wave speeds for the three waves that may be present in the model.

We may compare the instabilities in the two models described above with the instability in the most simple model of the Gates type. Figure 8 gives the e-folding times for $U_T$ = 25 m per s. It is seen that the smallest e-folding times are 0.5 days, and that the region of instability is about the same as in the balanced model. This statement is seen more clearly in Figure 9 where we display the e-folding time for the most general and the most simple model. The e-folding times for the classical 2-level, quasi-nondivergent model is given in Figure 10 for comparison. The relative position of the thermal streamfunction, the streamfunction for the 500 hPa level and the vertical velocity (omega) are shown in Figure 11 in such a way that the amplitudes of the streamfunctions and the vertical p-velocity are normalized to unity. It is seen that the maximum of the thermal streamfunction is lagging behind the streamfunction at 500 hPa in agreement with the observed structure of atmospheric waves. The wavelength used in these calculations is 5000 km.

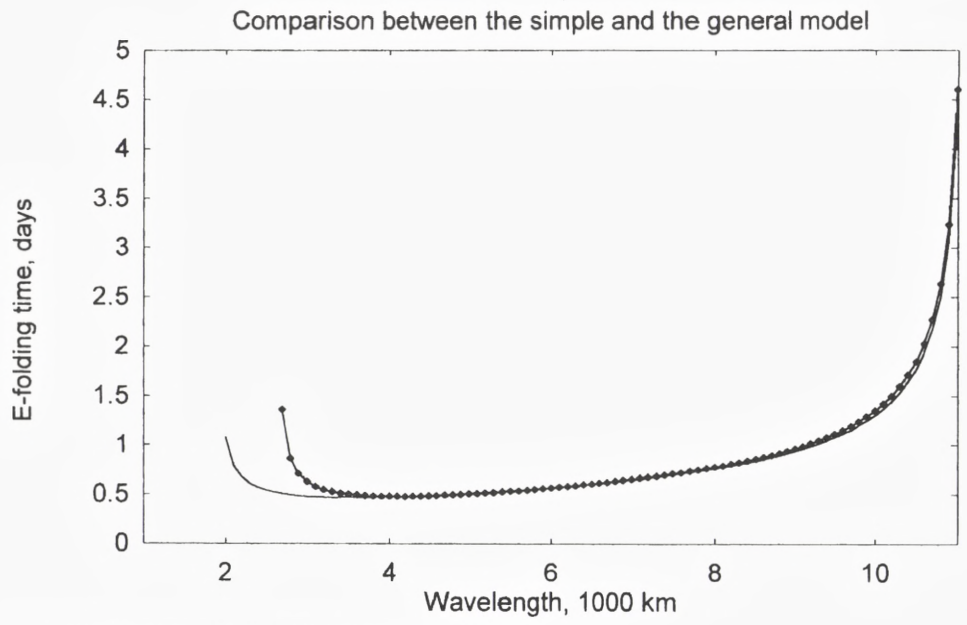


Fig. 9: E-folding time, days, for the general and the simple models.

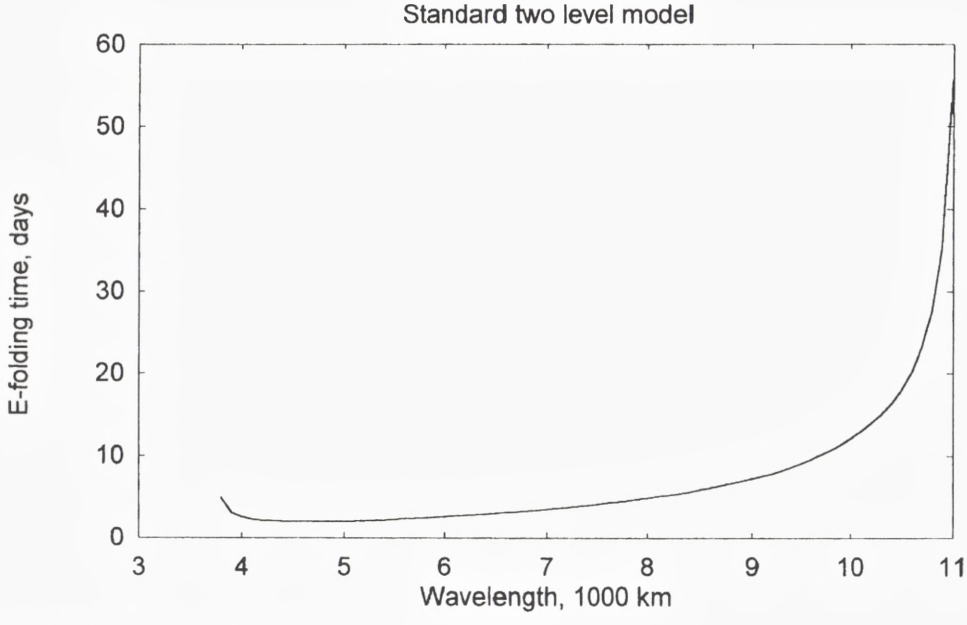


Fig. 10: E-folding time, days, for the standard two-level model.

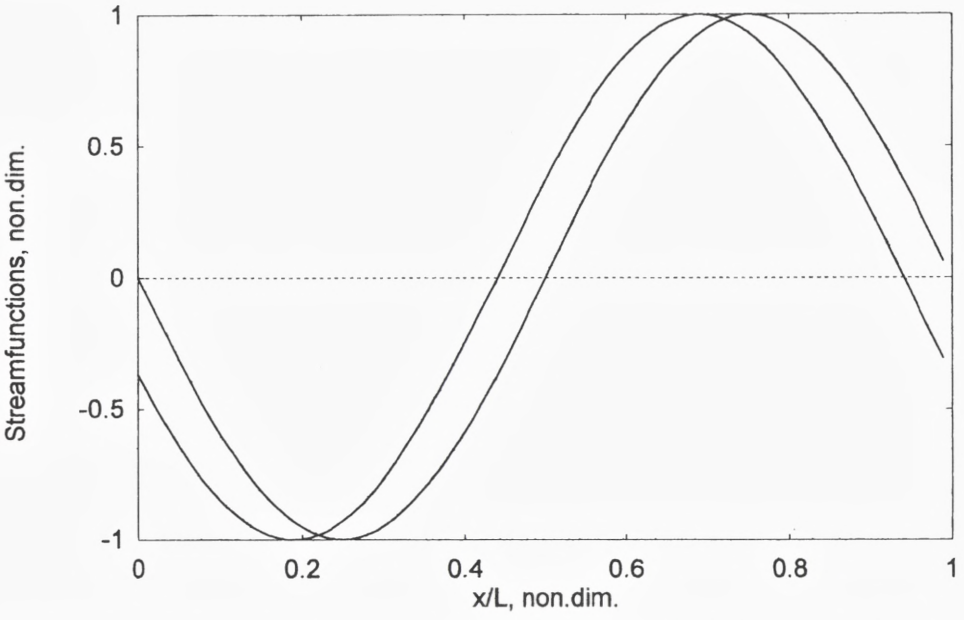


Fig. 11: The relative positions of the streamfunctions for the thermal field and the field at 500 hPa. Amplitudes are normalized to unity.

## 4. Consideration of the nonlinear aspects

As mentioned earlier the stability studies can only give the growth tendency in the unstable cases. The e-folding times are indicators of the speed of growth.

Observational studies of atmospheric energetics have shown that most of the time the energy flows from the zonal available to the eddy available potential energy. The eddy available potential energy is converted to eddy kinetic energy, and from the latter energy reservoir one finds a conversion to zonal kinetic energy. An exception to the described energy flow is the blocking situations, where the energy conversion between the eddy kinetic and the zonal kinetic energy in general changes direction. The conversion between the zonal available potential energy and the zonal kinetic energy is on average very small.

In the stability studies treated in Section 3 the basic zonal state is constant, and the growing disturbances will continue to grow. This is of course an unrealistic treatment, and we shall in this section consider a more realistic approach. Since it requires the use of nonlinear equations, we can no longer use an analytical approach and obtain the solutions in a closed form, but we have to use numerical integrations. In reality the growing waves will draw the energy from the zonal state.

In the general case they may receive the energy from the zonal available potential energy and the zonal kinetic energy, when we consider cases in which we observe a mixture of barotropic and baroclinic instability. This means naturally that these two forms of energy may decrease, but in the case treated in Section 3 the basic zonal state is constant, and the growing disturbances will continue to grow.

To be realistic the model should have variations of the tempeature and wind fields in the basic state with both pressure and respect to the meridional coordinate. One could use a model similar to the one designed by Phillips (1956), but since long integrations are required it may be a too slow process to make many long integrations of a grid point model. It was therefore decided to use an already existing low order model designed by Marcussen and Wiin-Nielsen (1999). The model uses the beta-plane, and it is a two-level model. The zonal state contains the winds as specified by two trigonometric components with wave numbers 2 and 4, while the eddies are defined by two meridional components with wave number 1 and 3. This choice gives interactions between the components. The eddy components have a variation in the west-east direction characterized by the sine and cosine components with a single west-east wave number, which may vary from case to case. The model may therefore be called a twelve component model. The reader may find the details in the publication mentioned above including the equations.

In the general case the model has both heating and dissipation which may act on all components. On the other hand, the user may also select to have heating in the meridional direction only. It was decided to investigate the cases of interest by defining the heating and dissipation and to make integrations of the model equations by starting from the state of rest. We would then expect that the zonal heating with heating to the south and cooling to the north will increase the temperature gradient in the meridional direction and thus also create an increasing wind field with both horizontal and vertical variations. When the critical level has been passed we should expect that the waves would start to grow drawing the energy from the zonal state and thus decreasing the zonal energies for both the available potential energy and the kinetic energy. At some point the conditions for wave growth will vanish, and as the eddy energies decrease we will expect that the zonal energies increase again to a state where wave growth can start once more. The experiments will thus also give an estimate of the order of magnitude of the life time of a wave with a specified wavelength.

After some experiments it was seen that a useful answer can be obtained by making integrations for 50 to 100 days. In the remaining part of this section we shall consider some examples.

Figure 12 shows the time variation of the zonal available potential energy and the zonal kinetic energy over 100 days in an experiment with forcing on the largest meridional scale only ($h_2 = 8.0 \times 10^{-3}$ J per kg and sec). We notice that these energies

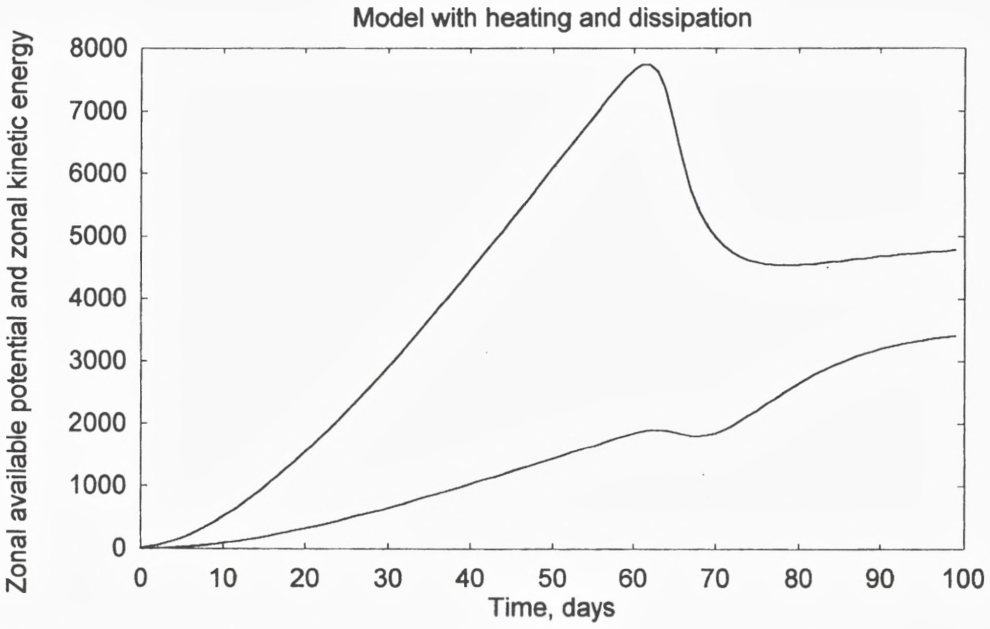


Fig. 12: The zonal available potential energy and the zonal kinetic energy as function of time.

increase for the first part of the integration, and that they are essentially in phase with each other. Later in the integration when they grow again we observe that they gradually come out of phase. Figure 13 shows the variation in time of the two forms of eddy energy. The upper line is the eddy available potential energy and the lower the eddy kinetic energy. In the beginning we notice a moderate growth where the maximum in the eddy kinetic energy appears a little after the maximum in the eddy available potential energy. When the development of the waves become more intense after more than 100 days of integration one can see that the growth of the eddy kinetic energy comes after the growth of the eddy available potential energy by a few days (not included in the figure).

While all the energy generations, conversions and dissipations may be computed it will suffice for the present purpose to note that an agreement exists between the energetics of the model and the energetics based on observational studies (Wiin-Nielsen and Chen, 1993) with respect to directions and orders of magnitude. The result of the long nonlinear integration may be seen in Figure 14 showing the streamfunctions at the upper (250 hPa) and the lower (750 hPa) levels for a wavelength of 5000 km. It is seen from this figure that the final shape of the wave has the typical 'Ω' shape indicating a wave of the blocking type, and that the wave

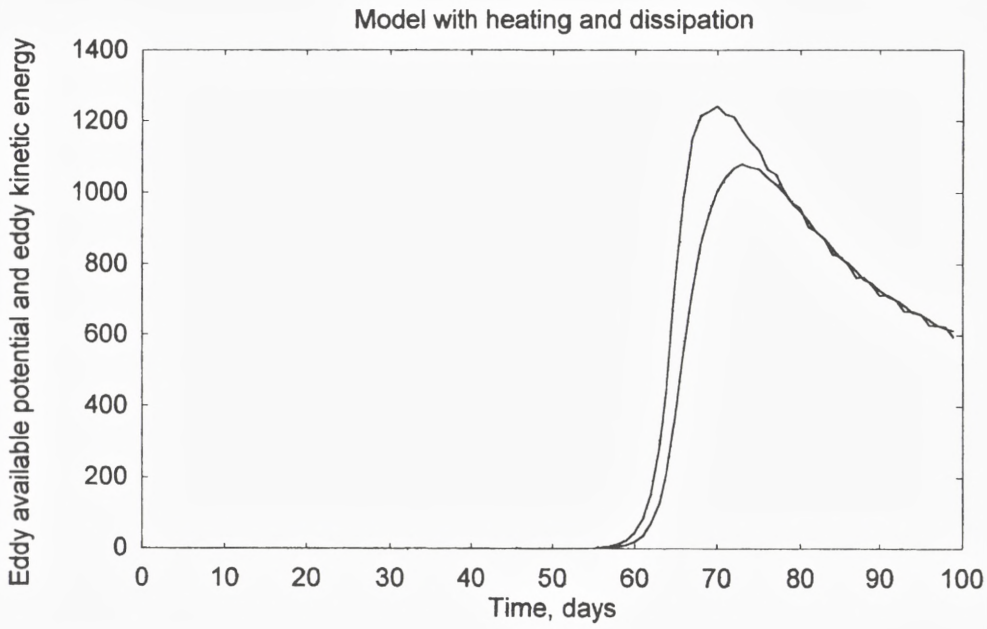


Fig. 13: The eddy available potential energy and the eddy kinetic energy as functions of time.

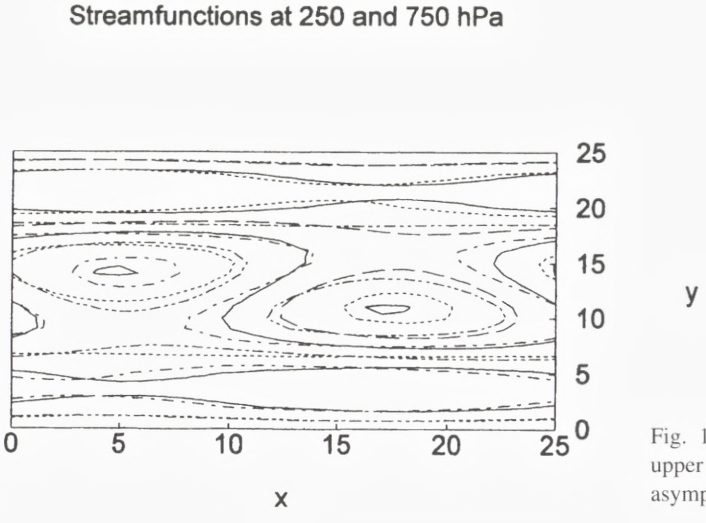


Fig. 14: The streamfunctions at upper and the lower levels in the asympotic steady state.

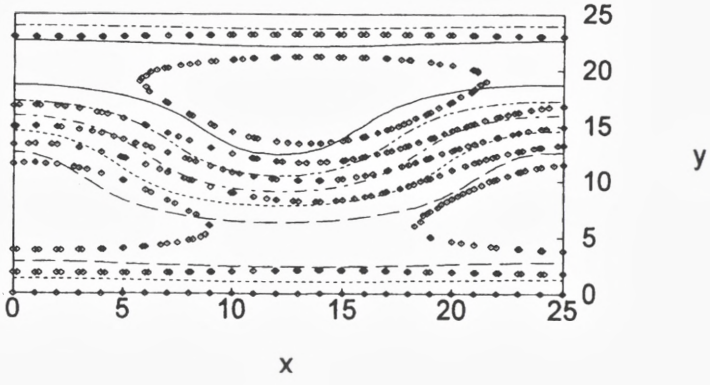


Fig. 15: As Figure 14, but at 60 days.

has a vertical slope from east to west which is also characteristic for the observed wave.

A second experiment is undertaken in which the heating as before is limited to have a variation on the largest scale in the meridional direction only ($h_2 = 3.4 \times 10^{-3}$ J per kg and sec). The purpose of the experiment is to describe the development of the first waves, to determine the time scale for this wave and to use the computations of the standard energy conversions to test whether or not they agree with the results of observational studies.

Figure 15 contains the streamfunctions at the two levels after an integration for 60 days. The solid line is the streamfunction at the upper level (250 hPa), while the dotted curve is for the lower level (750 hPa). One notices the slope from east to west in the vertical direction, and also that closed isolines are present at the lower level, but not at the upper level. The phase difference is clearly seen on the figure. The similarity with the typical structure of the waves in the troposphere is apparent.

## 5. The stability analysis of the primitive three level model

A three-level model based on the primitive equations can be formulated. To include the beta-effect it is necessary to use the vorticity equation and the divergence equations. In addition we need the thermodynamic equation and the continuity equation. The basic variables are the streamfunction, the velocity potential, the geopotential and the vertical velocity. In the three level model we use the vorticity and the divergence equations at levels 1, 3 and 5 and the remaining equations at the levels 2 and

4. As a final step we may add the equation for the vertical velocity at the 1000 hPa level as discussed earlier, or it may be assumed that $\omega = 0$ at level 6.

In this section we shall disregard heating and friction. The equations are linearized using a basic state in which the three zonal winds ($U_1$, $U_3$, $U_5$) and the two static stability parameters ($s_2$, $s_4$) depend on pressure only. It is convenient to define the two thermal winds in the model by $U_{T2} = U_1 - U_3$ and $U_{T4} = U_3 - U_5$. The stability analysis is carried out, and it is then possible to determine the e-folding time as a measure of the instability. The results for various cases will be discussed below.

In the first examples we use $U_{T2} = U_{T4} = 10$ m per s and $s_2 = 5.31 \times 10^{-6}$ and $s_4 = 1.91 \times 10^{-6}$ both measured in the unit: $m^4\ s^2\ kg^{-2}$. Figure 16 shows the e-folding times for the short waves in an interval from 2400 km to 6300 km with e-folding times as low as 2 days. Figure 17 is concerned with the long waves. Instability is found from 8000 km to 28000 km, but the e-folding times are large with a minimum of about 8 days. It should be mentioned that three instabilities are present for the long waves. The e-folding times for all three instabilities are shown in Figure 18. In the text to follow only the largest instability, i.e. the lower curve, will be considered.

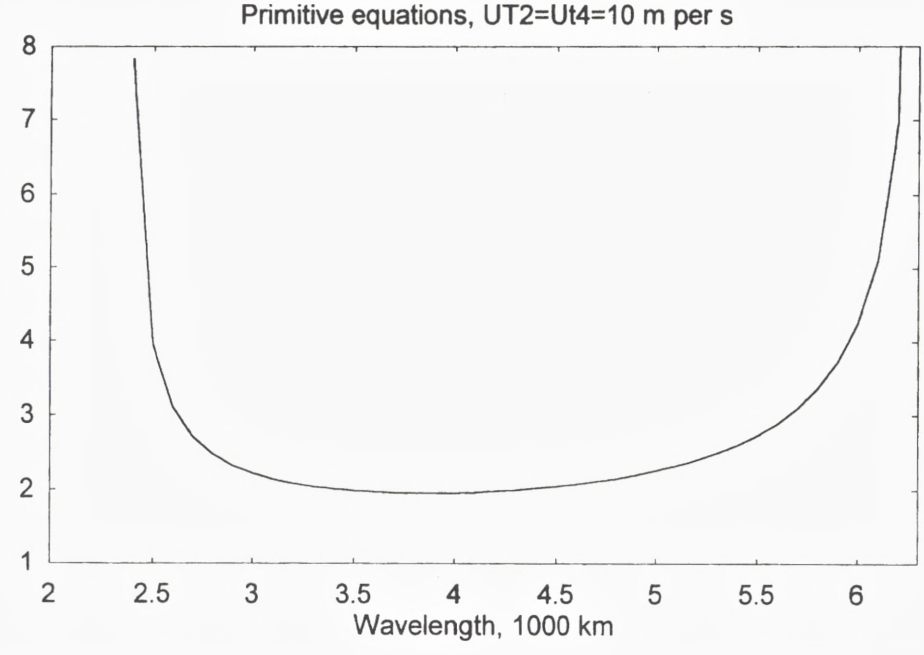


Fig. 16: The e-folding times in days for the shorter waves using the primitive equation model.

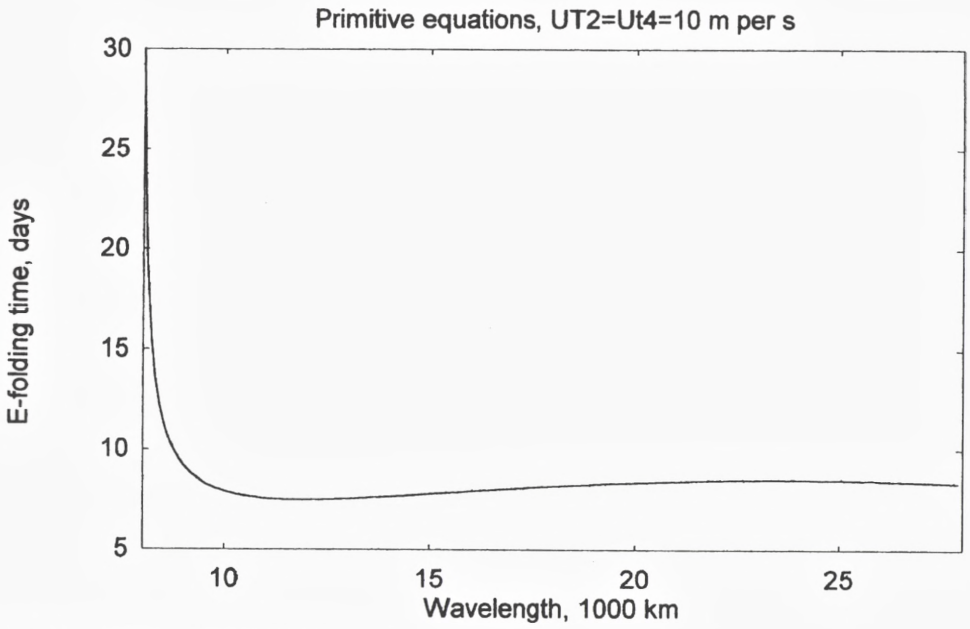


Fig. 17: As Figure 16, but for long waves.

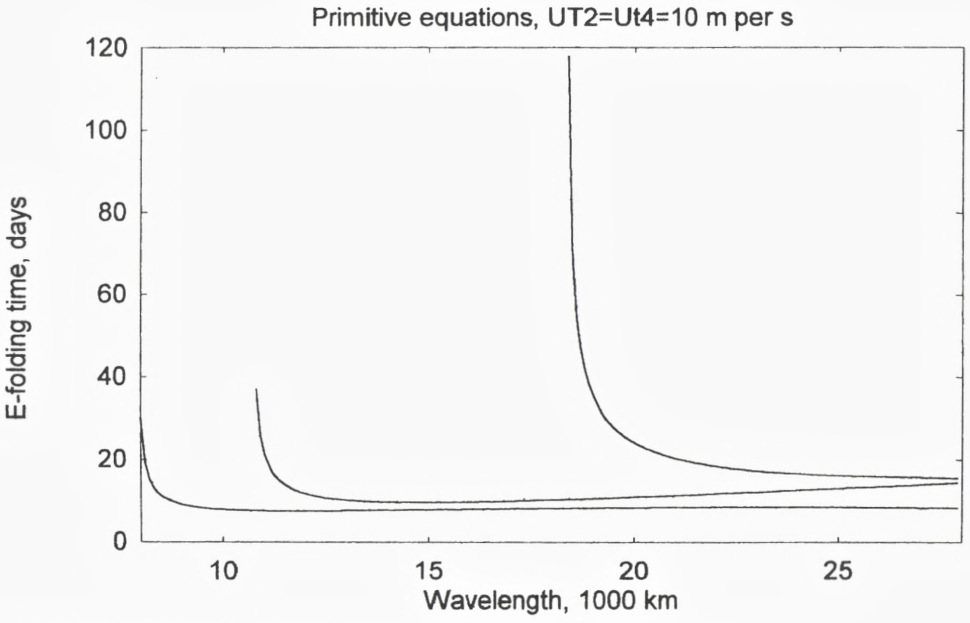


Fig. 18: The e-folding time in days for the very long waves including all unstable waves.

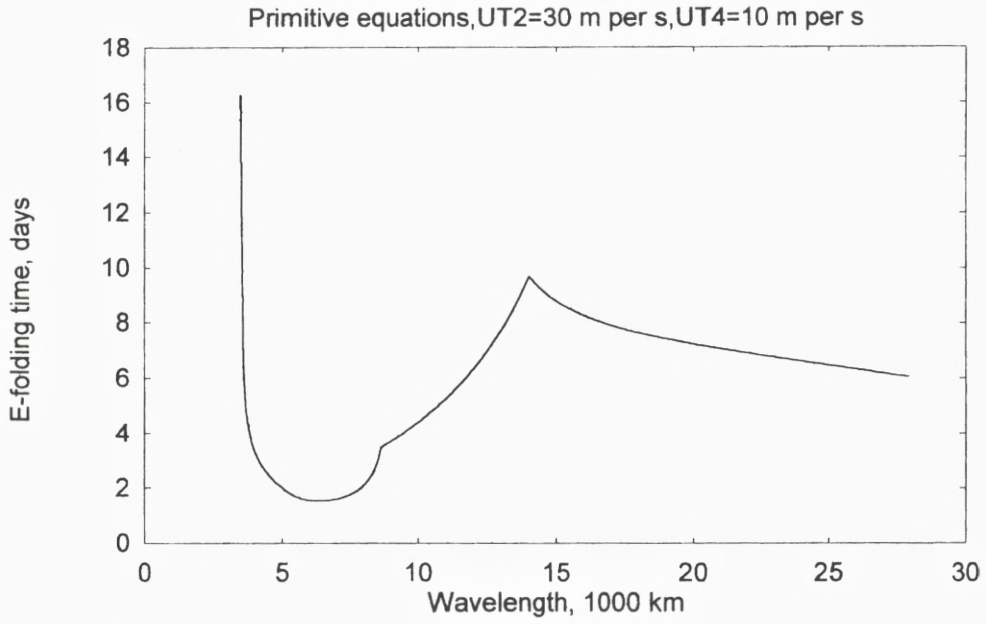


Fig. 19: The e-folding time in days for the case with $U_{T2}$ = 30 m per s and $U_{T4}$ = 10 m per s.

Figure 19 is based on a basic state with the same values of $s_2$ and $s_4$ as given above, but with $U_{T2}$ = 30 m per s and $U_{T4}$ = 10 m per s. The larger wind shear in the upper layer results in instability from about 3000 km to 28000 km, but the discontinuities in the slope of the e-folding curve indicate that different mechamisms may be at work. In Figure 20 we have used $U_{T2}$ = 10 m per s and $U_{T4}$ = 30 m per s and no change in the static stability parameters. Once again, the instability covers a large region from about 2000 km to 28000 km, but for this less realistic variation of the zonal wind in the basic state the e-folding times are very small for the shorter waves. The very long waves have also smaller e-folding times (about 3.2 days). The reason for this behavior is that the larger wind shear appears together with the smaller static stability parameter.

In the next experiment we use a value of 10 m per s for the vertical wind shears and replace the two different values of $s_2$ and $s_4$ by a single numerical value of $3.61 \times 10^{-6}$ $m^4$ $s^2$ $kg^{-2}$ which is the average of the first numerical values of the static stability parameters. Figure 21 shows the complete result. Instability is found only at the shorter waves from 4000 to 6300 km. It appears therefore that the vertical variation of the static stability parameter is a necessity for instability of longer waves. In the following section we shall investigate this tentative conclusion using a quasi-nondivergent model.

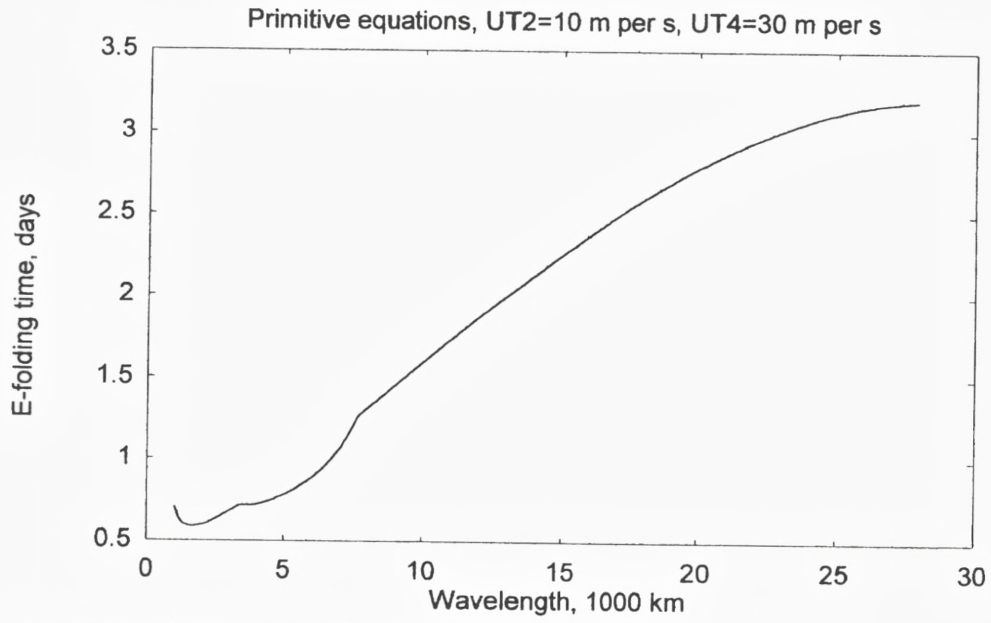


Fig. 20: The e-folding time in days for the case with $U_{T2}$ = 10 m per s and $U_{T4}$ = 30 m per s.

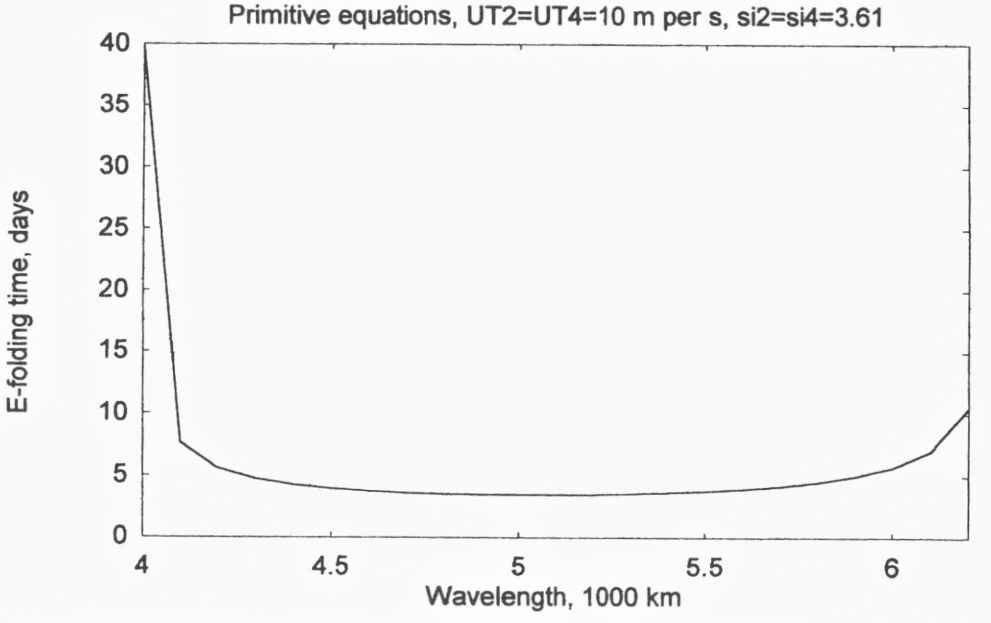


Fig. 21: The e-folding times, when the two stability parameters are equal to $3.61 \times 10^{-6}$ $m^4$ $s^2$ $kg^{-2}$. Instability is present only for the shorter waves.

## 6. Three-level, quasi-nondivergent model

It has been seen that only the so-called general model with a vertical variation of the static stability parameter shows baroclinic instability for very long waves, while the so-called balanced model shows baroclinic instability for the shorter waves only. One may therefore ask if the instability of the very long waves requires a variation with respect to pressure of the static stability parameter. The standard two-level, quasi-nondivergent model with a constant value of the stability measure has only instability for the shorter waves. The most simple model permitting a vertical change of the stability measure is thus the three-level, quasi-nondivergent model. This model has been investigated for baroclinic instability by the author. The basic equations for the model may be found in the paper by Wiin-Nielsen (1989). The parameter in question is for quasi-geostrophic models defined as given in (6.1).

$$\sigma = -\alpha \frac{\delta(\log\theta)}{\delta p} \tag{6.1}$$

The vertical variation of σ has been investigated (Wiin-Nielsen, 1991). The stability parameters have the same values as used in Section 5. We shall first demonstrate that the quasi-nondivergent model has instabilities similar to the model based on the primitive equations.

Figure 22 shows the computed e-folding time as a function of wavelength for the shorter waves in a model with $U_{T2}$ = 30 m per s and $U_{T4}$ = 10 m pers. Instability is found from 2300 km to almost 9000 km. Figure 23 indicates that instability of a weak nature is present for the long waves from about 12600 km. In the next calculation with $U_{T2}$ = 10 m per s and $U_{T4}$ = 30 m per s we find for the shorter waves instabilities from 2000 to 9000 km (se Figure 24). For the long waves the e-folding time are shown in Figure 25. Weak instabilities are present. After these preparations confirming that also the quasi-nondivergent model indicates instabilities for the long waves we turn to the special case where the values of both $s_2$ and $s_4$ are equal to $3.61 \times 10^{-6}$ $m^4$ $s^2$ $kg^{-2}$. Figure 26 shows also for the quasi-nondivergent model that the instabilities are restricted to the shorter waves.

In section *2b* we have applied the two-level model to get an estimate of the velocity of the thermal wave and found that the order of magnitude is 190 m per s. While dealing with three-level models we may use the model to determine the velocities of the thermal waves. As in the simple case of two levels we need the equations of motion, the thermodynamic equations and the continuity equations. Applying the equations of motion at the three levels marked 1, 3 and 5 we get the equations listed in (6.2).

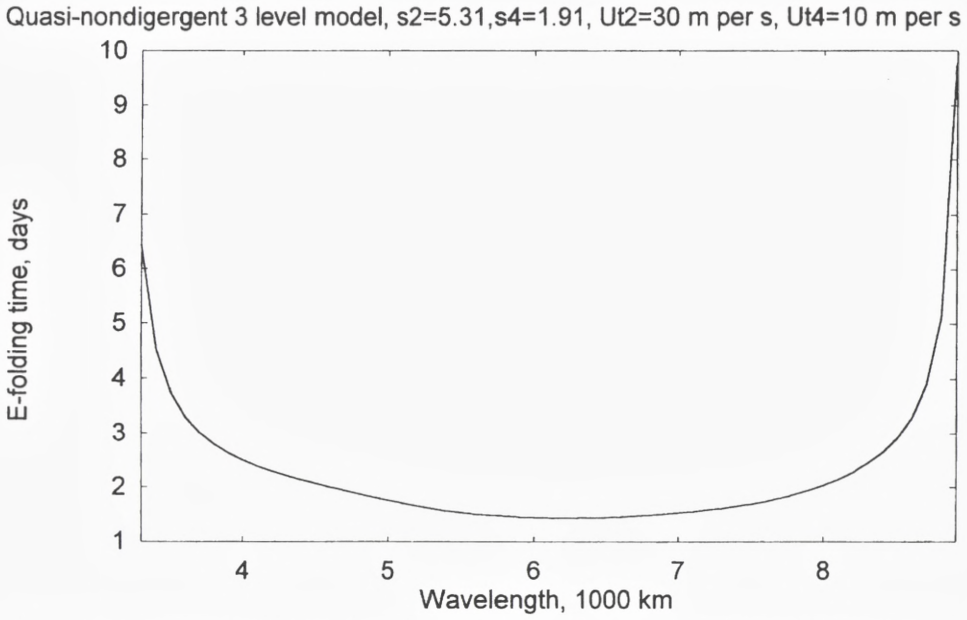


Fig. 22: The e-folding times in days for the three level quasi-nondivergent model for the shorter waves.

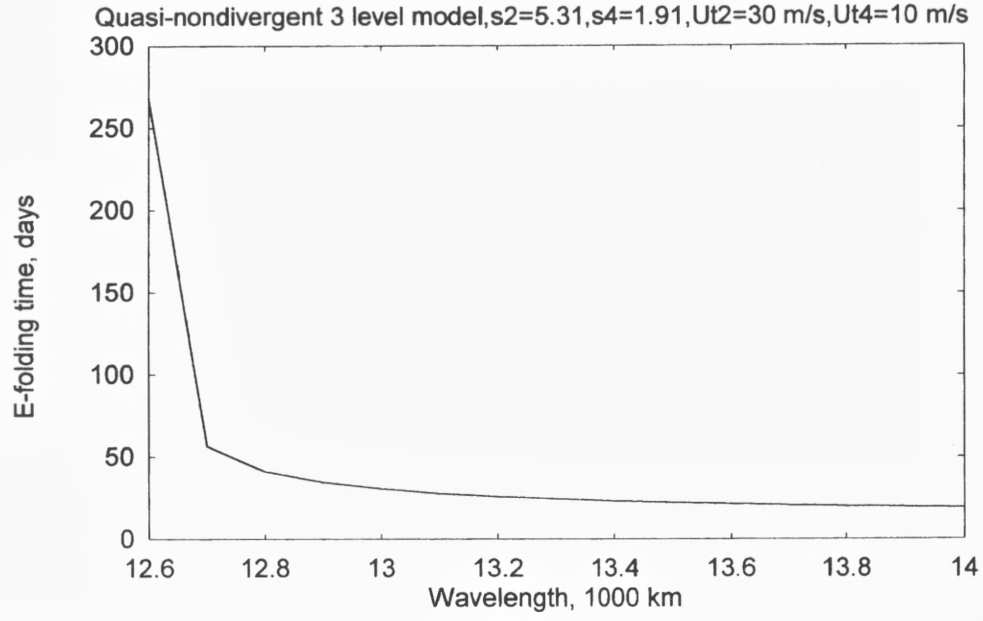


Fig. 23: The e-folding times in days for the three level quasi-nondivergent model for the longer waves.

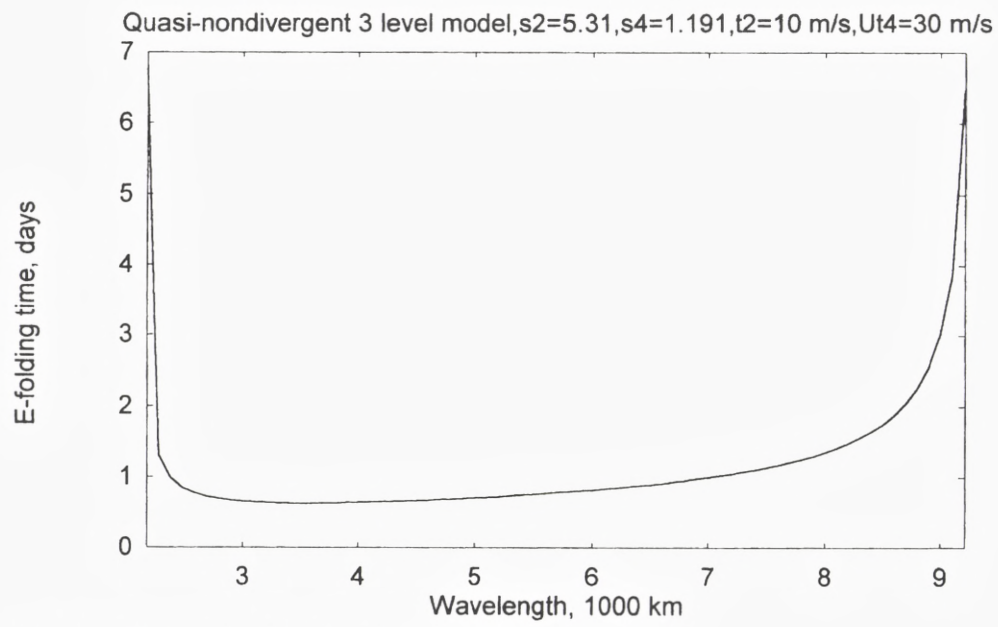


Fig. 24: As Figure 22, but with $U_{T2}$ = 10 m per s and $U_{T4}$ = 30 m per s.

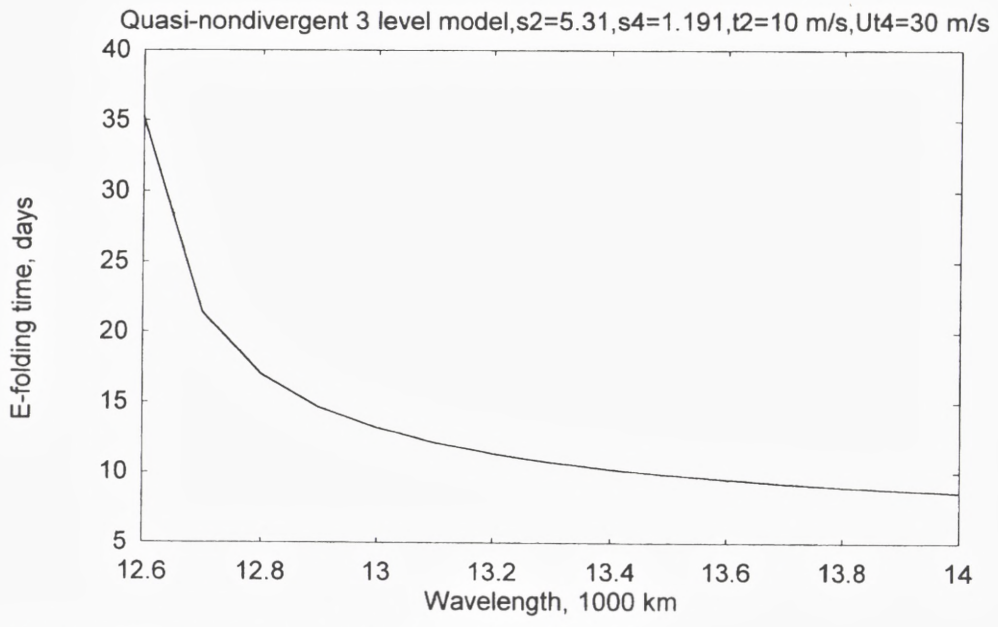


Fig. 25: As Figure 23, but with $U_{T2}$ = 10 m per s and $U_{T4}$ = 30 m per s.

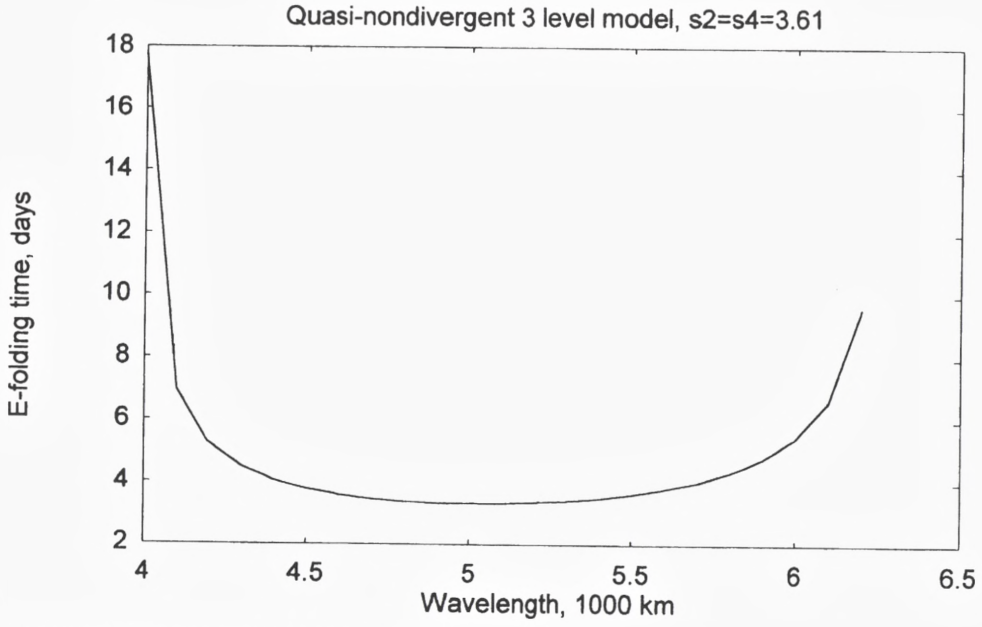


Fig. 26: E-folding time (days) for the case where $s_2 = s_4 = 3.61$.

$$\begin{aligned} \frac{\delta u_1}{\delta t} &= -\frac{\delta \Phi_1}{\delta x} \\ \frac{\delta u_3}{\delta t} &= -\frac{\delta \Phi_3}{\delta x} \\ \frac{\delta u_5}{\delta t} &= -\frac{\delta \Phi_5}{\delta x} \end{aligned} \tag{6.2}$$

The thermodynamic equation is used at levels 2 and 4 with the result given in (6.3).

$$\begin{aligned} -\frac{\delta(\Phi_1-\Phi_3)}{\delta t} + \sigma_2 P \omega_2 &= 0 \\ -\frac{\delta(\Phi_3-\Phi_5)}{\delta t} + \sigma_4 P \omega_4 &= 0 \end{aligned} \tag{6.3}$$

We apply finally the continuity equation at level 1, 3 and 5 with the results shown in (6.4).

$$\frac{\delta u_1}{\delta x} + \frac{\omega_2}{P} = 0$$

$$\frac{\delta u_3}{\delta x} + \frac{\omega_4 - \omega_2}{P} = 0 \qquad (6.4)$$

$$\frac{\delta u_5}{\delta x} + \frac{\omega_4}{P} = 0$$

By adding the three equations in (6.4) we get zero which of course says that the vertical average of the divergence vanishes in agreement with the boundary conditions that the vertical p-velocity in the model is zero at the top and the bottom of the atmosphere.

The eight equations are reduced to three equations by first eliminating the vertical p-velocities, i.e. substituting from (6.4) into (6.3). Thereafter we eliminate the geopotentials. The final three equations are given in (6.5).

$$\frac{\delta^2 u_1}{\delta t^2} - \frac{\delta^2 u_3}{\delta t^2} = \sigma_2 P^2 \frac{\delta^2 u_1}{\delta x^2}$$

$$\frac{\delta^2 u_3}{\delta t^2} - \frac{\delta^2 u_5}{\delta t^2} = \sigma_4 P^2 \frac{\delta^2 u_5}{\delta x^2} \qquad (6.5)$$

$$\frac{\delta u_1}{\delta x} + \frac{\delta u_3}{\delta x} + \frac{\delta u_5}{\delta x} = 0$$

The normal form of the perturbations are introduced in (6.5) resulting in three linear equations. Setting the determinant equal to zero we obtain the fourth degree equation given in (6.6).

$$3c^4 - 2\,(\sigma_2 P^2 + \sigma_4 P^2)\, c^2 + \sigma_2 \sigma_4 P^4 = 0 \qquad (6.6)$$

The solutions of (6.6) are calculated using the same values of the two static stabilities as employed in the previous program recalling also that P = $^1/_3$ $10^5$ P. The numerical values are 72.9 m per s and 42.1 m per s. It is thus seen that the thermal waves will move with considerable speeds in the models permitting a vertical variation of the static stability.

## 7. General description of inertial motion

The very brief description of inertial waves found in Section 2a uses a constant

value of the Coriolis parameter. If this assumption is maintained, the trajectory of a particle influenced only by the Coriolis force will be a circle as demonstrated in elementary meteorological textbooks (see for example Wiin-Nielsen, 1973) where it also is found that the radius of the circle becomes $V_o/f_o$ where $V_o$ is the initial velocity. It was pointed out in Section 2 that inertial motion seldom is seen in the real atmosphere because it requires a vanishing pressure force. However, inertial motion is important for many other applications where a calculation of the path of a body in the gravity field of the Earth is required. It may thus be of interest to determine such trajectories.

Assume for example that a particle at the initial time starts from a given point on the spherical Earth with a velocity $V_o$ from south to north. As it moves to the north it will experience an increasing Coriolis force ($f = 2\ \Omega \sin(\varphi)$). The particle will therefore turn more to the right than at the initial time. When it goes through the initial latitude, it will start to experience a smaller Coriolis force, and it will then turn less to the right. This means that the particle will not return to the original longitude, but will have moved to the west. This qualitative description can be verified by integrating the equations of motion on the sphere. The equations of motion for the problem are shown in (7.1) together with the equations necessary to provide the new positions in longitude and latitude.

$$\begin{aligned}
\frac{du}{dt} &= v\sin(\varphi)\,(2 + \frac{u}{\cos(\varphi)}) \\
\frac{dv}{dt} &= u\sin(\varphi)\,(2 + \frac{u}{\cos(\varphi)}) \\
\frac{d\lambda}{dt} &= \frac{u}{\cos(\varphi)} \\
\frac{d\varphi}{dt} &= v
\end{aligned} \tag{7.1}$$

The four equations are integrated numerically. Figure 27 shows an example where the initial position is at longitude 0 and latitude 45 with an initial velocity from south to north of 20 m per s. It is seen that the spiral motion gradually moves the particle further to the west. Figure 28 shows another case where the particle starts at the equator with a northward velocity of 20 m per s. The change in sign of the Coriolis parameter at the equator is apparent. Figure 29 shows the very special case where the particle comes back to the original position on the equator.

It is also possible to calculate the trajectory for three-dimensional, inertial

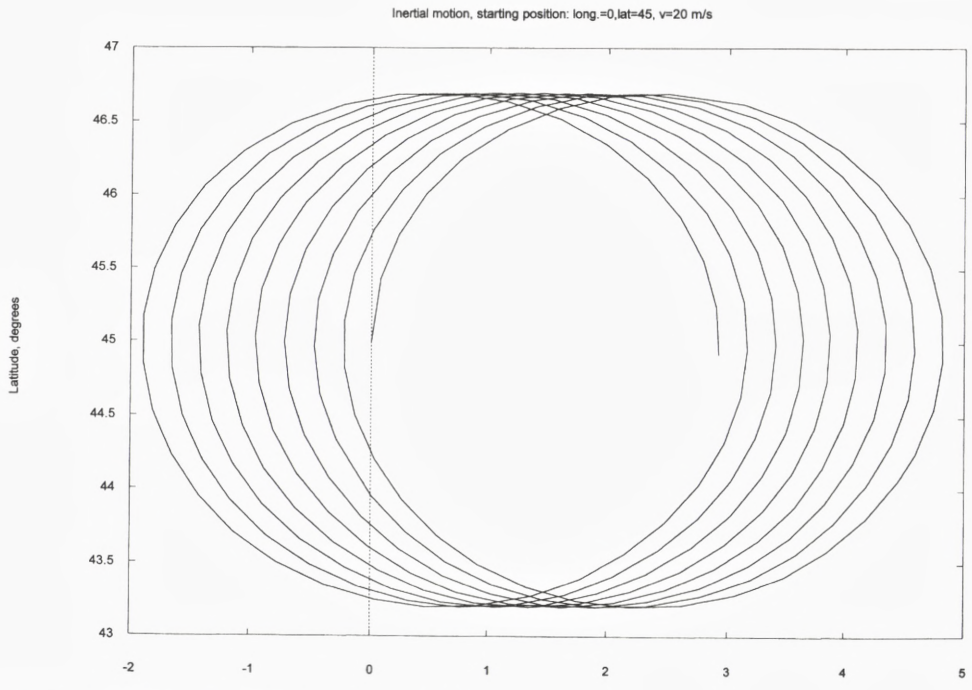


Fig. 27: Inertial motion starting from $\lambda = 0$, $\varphi = 25$, v= 20 m per s.

motion. An example will be shown. We consider a particle leaving the surface of the Earth at time t = 0 with an initial vertical velocity of 1000 m per s. We use in this example cartesian coordinates. In the equations for the vertical components of the velocity and the position we pay attention to gravity, (g = 9.807 m per $s^2$). The three equations of motion are given in (7.2).

$$\frac{du}{dt} = f_o v - e_o w$$

$$\frac{dv}{dt} = -f_o u \qquad (7.2)$$

$$\frac{dw}{dt} = e_o u - g$$

$$f_o = 2\Omega\sin(\varphi_o)\ ;\ e_o = 2\Omega\cos(\varphi_o)$$

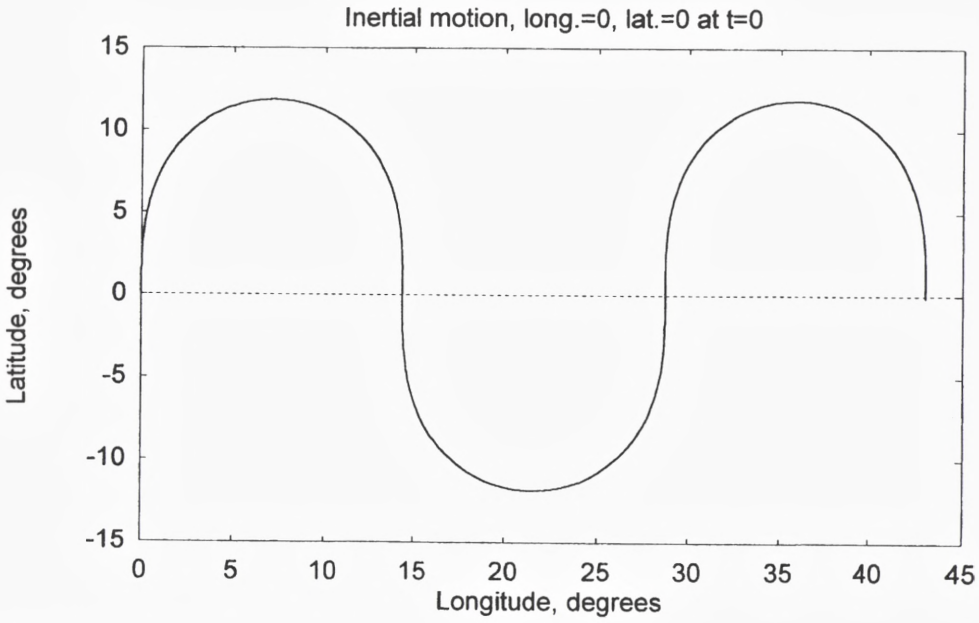


Fig. 28: Inertial motion starting from $\lambda = 0$, $\varphi = 0$, v=20 m per s.

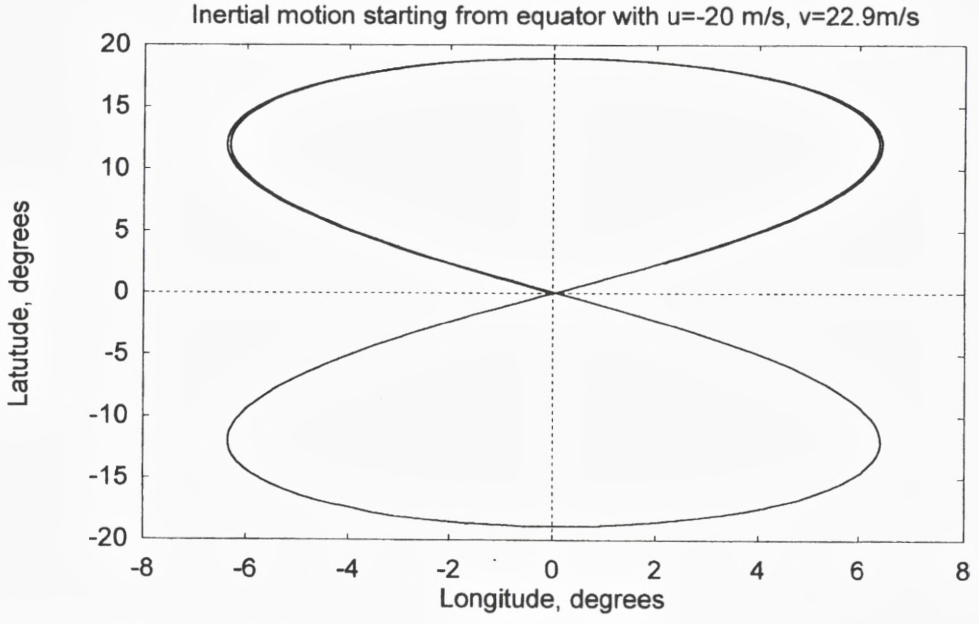


Fig. 29: Inertial motion starting from $\lambda = 0$, $\varphi = 0$, u= – 20 m per s and v = 22.9 m per s.

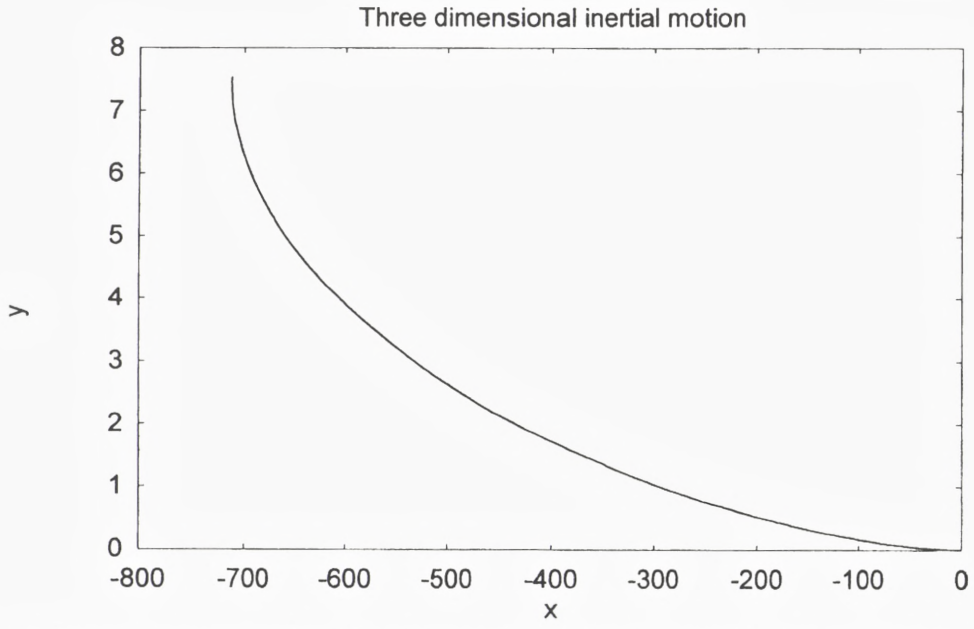


Fig. 30: The horizontal projection of the trajectory of the three-dimensional inertial motion starting from x = y = z = 0, u = v = 0, w = 1000 m per s.

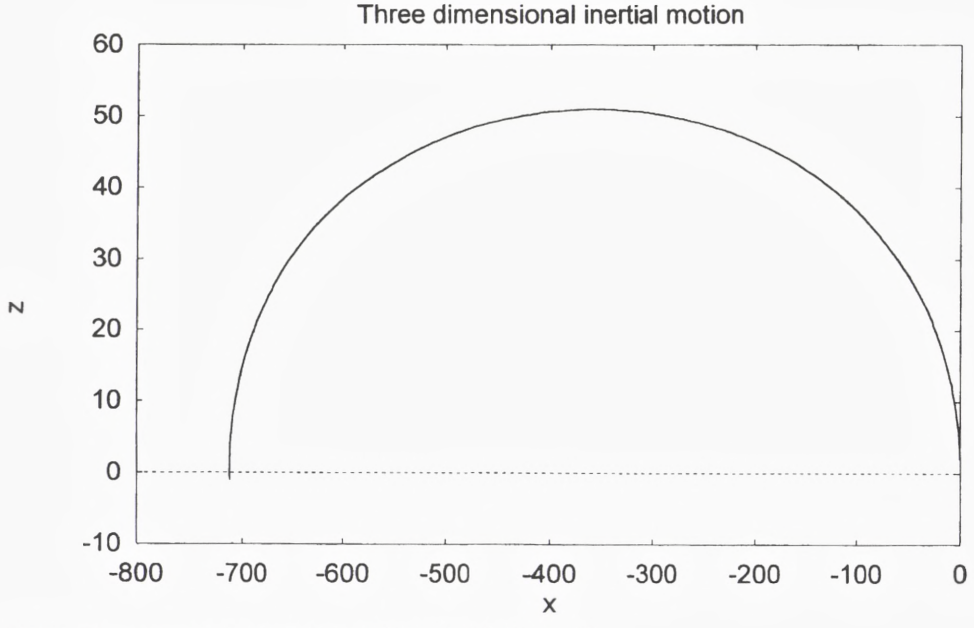


Fig. 31: The (x,z) trajectory for the case illustrated in Figure 30.

In addition we have the definitions of the three velocity components giving six equations to integrate. The integrations are continued to the time when the particle has landed on the Earth.

Before the presentations of the result one may consider the type of three-dimesional trajectory that can be expected. First of all, during the flight of the particle the Earth will move from west to east indicating that the particle will hit the surface of the Earth to the west of the starting point. However, the Coriolis force will as usual get the particle to turn to the right in the Northern Hemisphere, so the particle should land to the north of the starting position.

Figure 30 shows the (x,y)-trajectory with both coordinates given in m. The particle returns to the surface of the Earth a little more than 700 m to the west and about 7.5 meters to the north. Figure 31 shows the height of the particle as a function of time. It is seen that the particle comes to a height of more than 50 km, but the Earth is reached again after about 200 s or a little more than 3 minutes.

The case has also been treated in spherical coordinates, but the results are essentially the same due to a very small displacement in the meridional direction.

## 8. General determination of the thermal wave speed

It is of interest to investigate a more general case than the two- or three-level models for the determination of the thermal wave speed. It has been pointed out that the static stability parameter according to observational studies in the troposphere varies as given in (8.1).

$$\sigma = \sigma_o \frac{p_o^2}{p^2} \tag{8.1}$$

The expression in (8.1) is approximately in agreement with an atmosphere with a constant lapse rate. Evaluating the static stability parameter by using the gas equation and the definition of the potential temperature the expression in (8.2) is obtained.

$$\sigma = -\alpha \frac{\delta(\log\theta)}{\delta p} = \frac{R^2 T}{g p^2} (\gamma_d - \gamma) \tag{8.2}$$

Since the variation of temperature in the vertical direction is much smaller than the variation of $p^2$, (8.2) is in reasonable agreement with (8.1). On the other hand, (8.1) cannot be used at the top of the atmosphere because the static stability goes to infinity as the pressure approaches 0. To obtain a more accurate determination of

the higher components of the thermal speed, it was decided to use (8.1) for the troposphere only with the assumption that the vertical p-velocity vanishes at the top pressure level (say, 250 hPa) and at 1000 hPa. Under these assumptions we may obtain an equation for the vertical p-velocity by eliminating all the other variables from the perturbation equations. This equation is given in (8.3).

$$p^2 \frac{d^2\omega}{dp^2} + \frac{\sigma}{c^2}\omega = 0 \tag{8.3}$$

We shall use the notation introduced in (8.4).

$$A = \frac{\sigma_o p_o^2}{c^2} \qquad B = (4A-1)^{1/2} \tag{8.4}$$

The solution of the differential equation in (8.3) may then be expressed as shown in (8.5).

$$\omega = p^{1/2}\,(C_1 \cos\,(B\log\,(p)) + C_2 \sin\,(B\log\,(p)) \tag{8.5}$$

We use first the boundary conditions that the vertical p-velocity is zero for $p = p_T$ and $p = p_o$. After some derivations it is found that the phase speed c is determined by the relation shown in (8.6).

$$c^2 = \frac{4\sigma_o p_o^2}{1 + \dfrac{n^2\pi^2}{\ln\left(\dfrac{p_o}{p_T}\right)^2}} \tag{8.6}$$

It is also possible to investigate the changes if the simple boundary condition of a vanishing vertical p-velocity at 1000 hPa is replaced by the boundary condition given in (8.7).

$$\omega = -\frac{p_o}{RT_o}\frac{\delta\Phi}{\delta t} \tag{8.7}$$

Substituting from the thermodynamic equation we may write (8.7) in the form shown in (8.8) and valid at 1000 hPa.

$$\frac{\delta\omega}{\delta p} = \frac{p_o}{RT_o}\sigma_o\omega \tag{8.8}$$

The basic solution of the omega-equation is the same as before, but applying (8.8) as the boundary condition we obtain a different expression from which the thermal wave speed may be determined. This equation is obtained by using (8.7) at the lower boundary, while the boundary condition at $p = p_T$ is $\omega = 0$ as before. The new equation for the phase speed may be written in the form shown in (8.9).

$$(1-2r_o)\sin\left(B\ln\left(\frac{p_T}{p_o}\right)\right) - 2B\cos\left(B\ln\left(\frac{p_T}{p_o}\right)\right) = 0$$
$$r_o = \frac{\sigma_o p_o^2}{RT_o} \tag{8.9}$$

The notation in (8.4) has been introduced in equation (8.9). The problem is thus to solve (8.9) for B whereafter the phase speed is determined. The solution of (8.9) has been obtained by numerical methods.

The positive values of the thermal wave speeds are shown in Figure 32 for the two boundary conditions discussed above and as a function of n. It is seen that the thermal wave speeds are quite small for the components with the larger values of n, and that the more correct boundary condition results in a slower motion of the thermal waves in analogy with the results obtained in section *2e*.

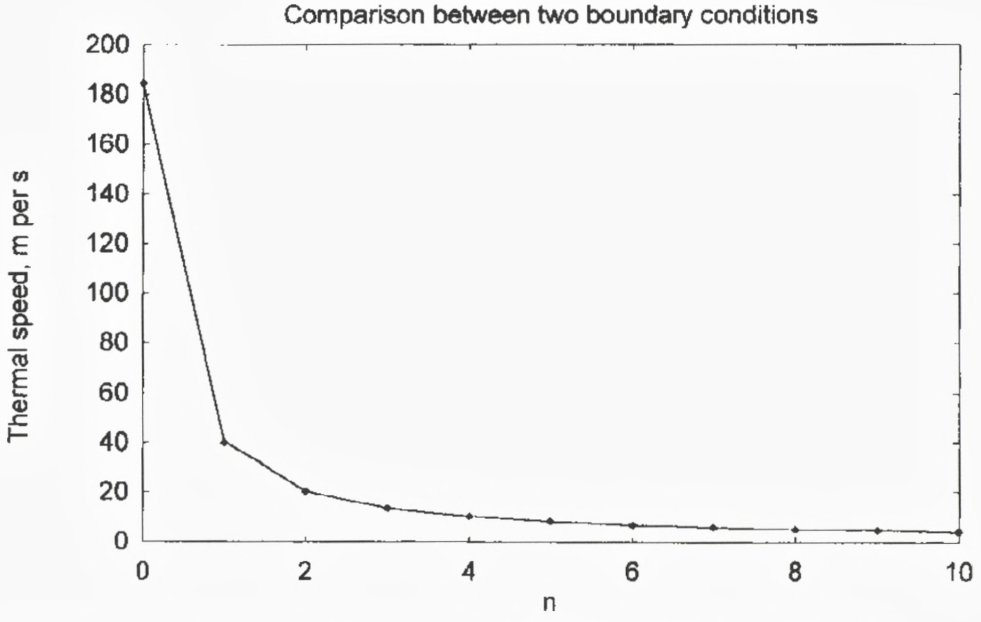


Fig. 32: Comparison between calculations using the two boundary conditions $w = 0$ and $\omega = 0$.

## 9. The shape of the waves

Most of the sections in the present paper contain the dependence on time of the amplitudes for the various wave components. In the present section we shall consider the behavior in space and time for the most general model without any basic zonal velocity. No instabilities are present in such a model. As before we consider the two level model with the lower boundary condition that $\omega = 0$ at $p_o = 1000$ hPa giving six equations, i.e. the vorticity equation at 500 hPa and the vorticity equation for the thermal flow, the divergence equations corresponding to the vorticity equations, and the geopotential at 500 hPa and for the thermal flow.

The six linear equations were integrated with respect to time from initial geostrophic conditions relating the streamfunction to the geopotential and a velocity potential computed from the solution of the quasi-geostrophic equation for the vertical p-velocity as discussed in section 8.

Figures 33, 34 and 35 show the two components of the streamfunction, the velocity potential and the geopotential as a function of time for 960 hours (40 days). Considering these figures it should be recalled that the streamfunction values are divided by $10^7$, the velocity potentials by $10^6$ and the geopotentials by $10^3$. It is seen that weak numerical noise appears in the velocity potential.

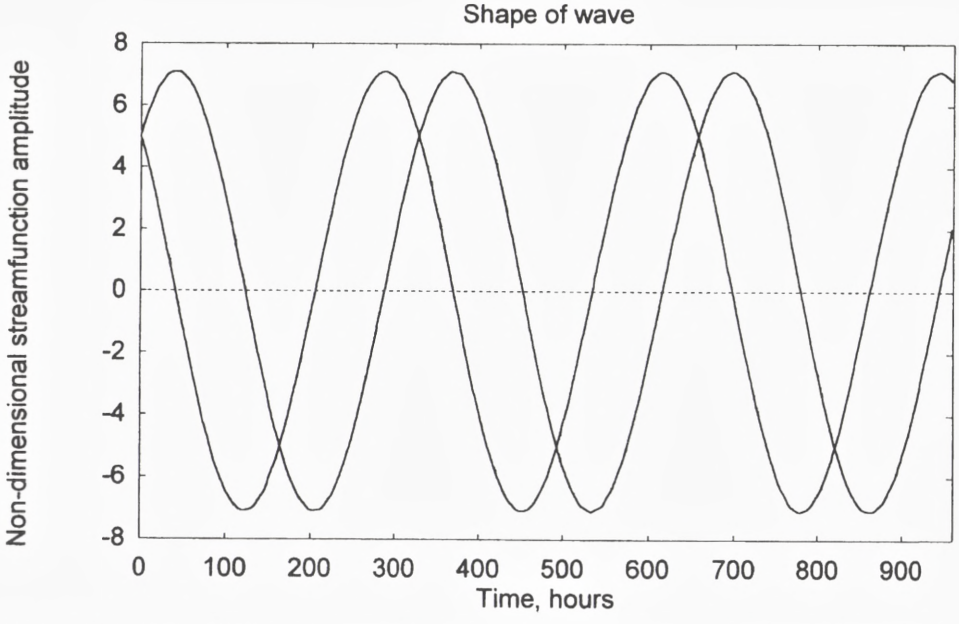


Fig. 33: The variation of the two components of the scaled streamfunction as a function of time (hours).

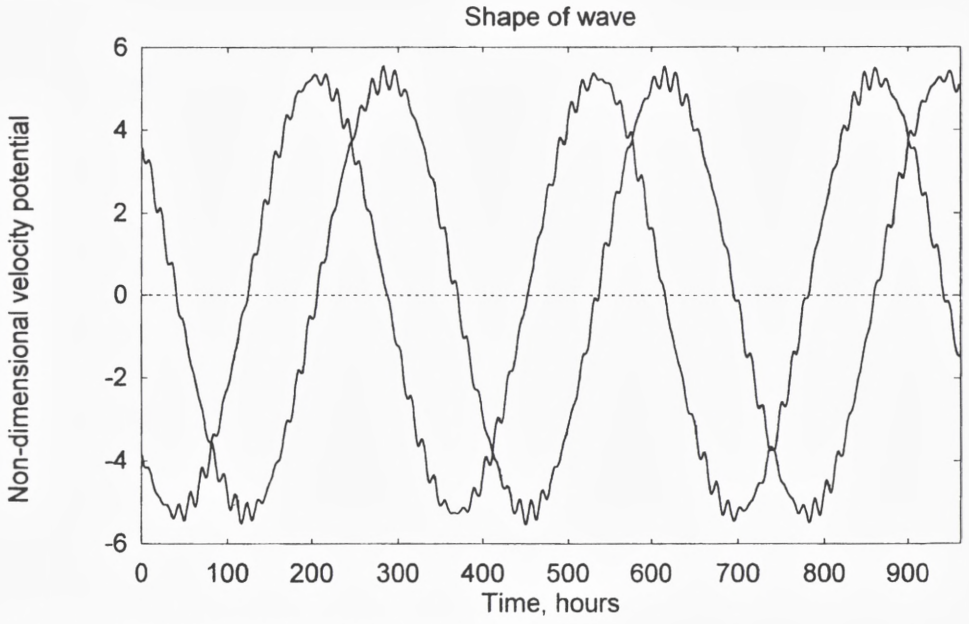


Fig. 34: As figure 33, but for the scaled velocity potential.

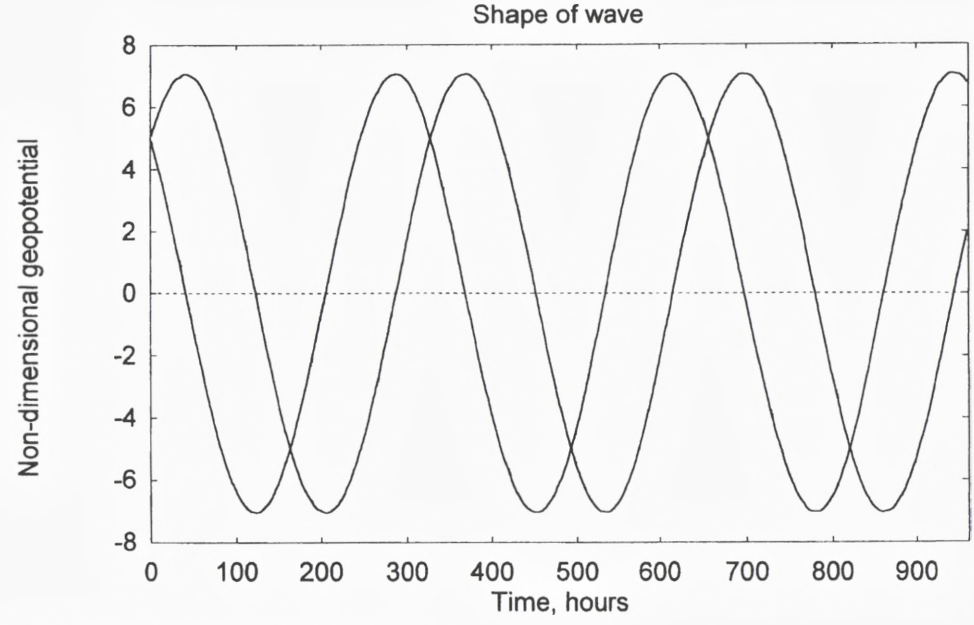


Fig. 35: As Figure 33, but for the geopotential.

Figure 36 shows the streamfunction, the velocity potential and the geopotential at 50 hours. It is seen that the geostrophic relation is present since the curves for the scaled streamfunction and the scaled geopotential coincide. The maximum value of the geopotential can easily be converted to a vertical p-velocity using the continuity equation. For a wavelength of 5000 km it is found that the magnitude of the vertical p-velocity is about 0.5 Pa $s^{-1}$ which is equal to a vertical velocity of about 7 cm $s^{-1}$. Figure 37 contains the same information as Figure 36, but at the time of 100 hours. It is clearly seen that the wave moves from east to west, i.e. c is negative. The distance between the maxima at 50 and 100 hours gives a measure of the negative wave speed. For L = 5000 km we find an averaged wave speed of –4.4 m per $s^{-1}$.

## 10. The boundary condition at $p = p_o$

The boundary condition at $p = p_o$ has been used in some of the problems in the present paper. The purpose of this section is to discuss the importance of this boundary condition. Needless to say, it is generally easier to handle the mathematics if one is

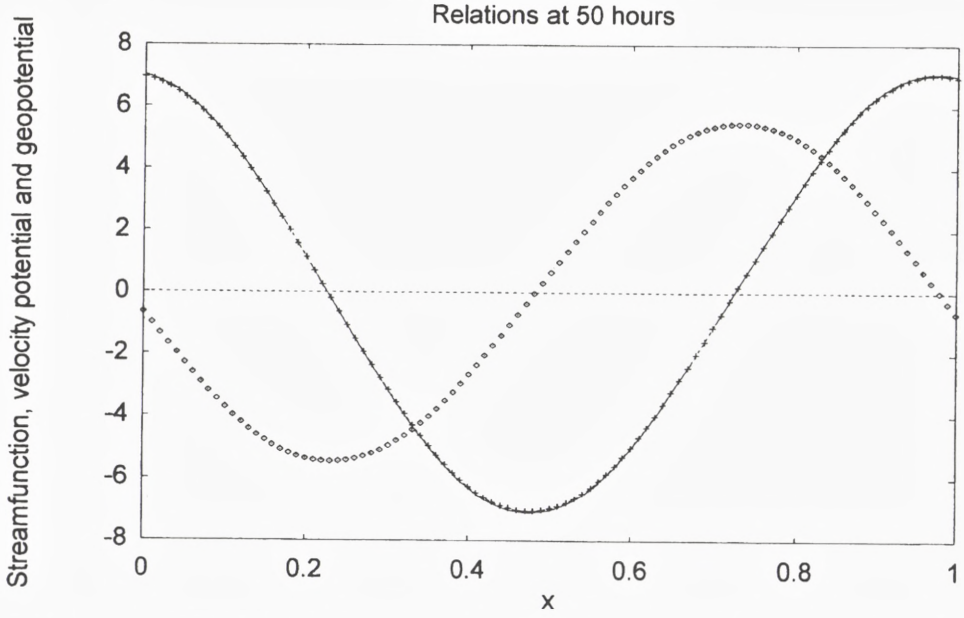


Fig. 36: Variations of the scaled velocity potential (dotted curve), the scaled streamfunction and the scaled geopotential as a function of x, the west-east coordinate, after integration over 50 hours.

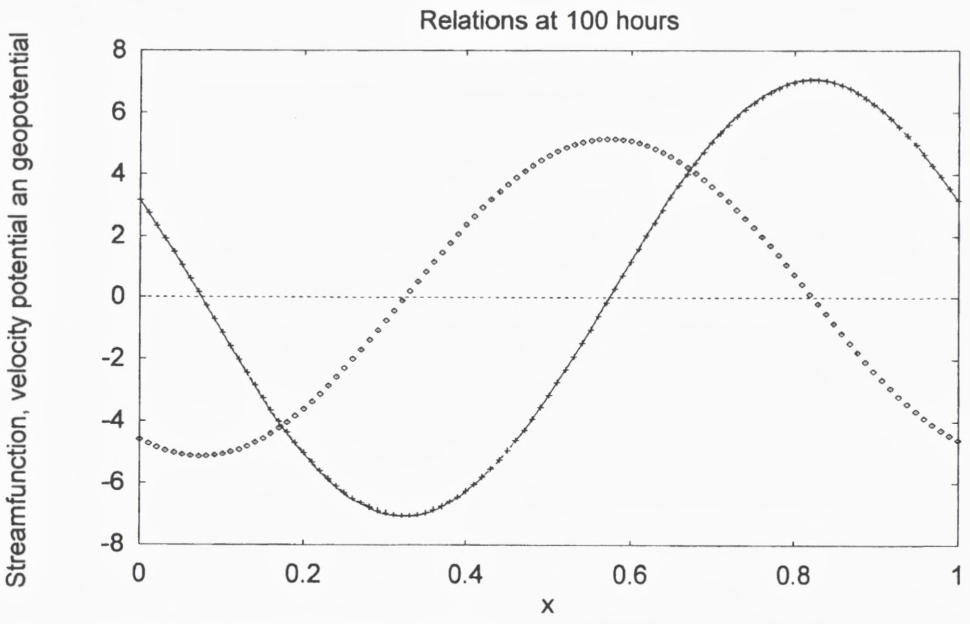


Fig. 37: As Figure 36, but after integration of 100 hours.

permitted to use the simple boundary condition: $\omega = 0$ at $p = p_o$. However, one cannot justify the simple condition in all cases. To illustrate this matter we return to the general case treated in Section 2. We use as before the primitive equations of motion supplemented by the thermodynamic equation and the continuity equation. The dependent variables are therefore the three components of the three-dimensional wind vector and the geopotential. As we have seen the perturbation equations without any basic velocity can be reduced to an equation for the vertical p-velocity in the form given in (10.1).

$$\frac{d^2\omega}{dp_*^2} + B^2\omega = 0 \tag{10.1}$$

The independent variable $p_*$ is the nondimensional pressure $p/p_o$. The dependent variable is the amplitude of the vertical p-velocity and the factor $B^2$ is defined as given in equation (10.2).

$$B^2 = \frac{C_T^2 (c + C_R)}{c\,((c + c_R)^2 - c_I^2} \tag{10.2}$$

The solution satisfying the upper boundary condition $\omega = 0$ is given in (10.3).

$$\omega = E\sin(Bp_*) \tag{10.3}$$

When the solution has to satisfy the simple boundary condition $\omega = 0$ at $p_* = 1$ we find $B = n\,\pi$. The equation for the phase speed is then as given in (10.4). This cubic equation has been solved earlier for c using the value $C_T^2 = 3.61 \times 10^4\ m^2\ s^{-2}$ giving a real speed for all values of the wavelength.

$$c^3 + 2C_R c^2 + (C_R^2 - C_I^2 - \frac{C_I^2}{(n\pi)^2})\,c - C_R\,\frac{C_I^2}{(n\pi)^2} = 0 \tag{10.4}$$

The more correct boundary condition at $p_* = 1$ is $w = 0$. As we have found this boundary condition may be written in the form displayed in (10.5).

$$\frac{d\omega}{dp_*} - \frac{RT_o}{C_I^2}B^2\omega = 0 \qquad p_* = 1 \tag{10.5}$$

To determine B in this case one has to solve the equation given in (10.6).

$$\cos(B) - \frac{RT_o}{C_I^2}\,B\sin(B) = 0 \tag{10.6}$$

The equation in (10.6) has been solved numerically. The first 10 roots are: B(0) = 0.6164, B(1) = 3.2742, B(2) = 6.3518, B(3) = 9.4709, B(4) = 12.6010, B(5) = 15.7357, B(6) = 18.8727, B(7) = 22.0110, B(8) = 25.1501, B(9) = 28.2898. We may compare these numerical values with the numbers $n\pi$ which are the equivalent numbers for the boundary condition $\omega = 0$. It is seen that B(n) is close to $n\,\pi$ for the larger values of n. The approximation is acceptable for n>1 because $B(2)/(2\,\pi) = 1.01$. For n = 1 we have $B(1)/\pi = 1.04$. With this value one will notice a real difference between the two profiles at $p_* = 1$. The solution B(0) = 0.6164 has no equivalent solution if the simple boundary condition is used. It is a very special solution starting by being zero at the top of the atmosphere and increasing to a maximum value of 0.58 at $p_* = 1$.

It should be mentioned that the results given above are based on a basic state of rest. When a zonal current in the basis state is introduced we may experience baroclinic instabilities, but the fast waves will still be present.

## 11. Geostrophic adjustment

The observed horizontal wind in middle and high latitudes is almost geostrophic. The reasons for this fact have been investigated by many meteorological authors from Rossby (1938) to Kuo (1997). All these investigations do not consider forcing and dissipation. A different approach to the problem of geostrophic adjustment has been presented by Wiin-Nielsen (2001). It is the purpose to simulate geostrophic adjustment in a model containing both forcing and dissipation. Starting from a state of rest the forcing will create atmospheric motion. The question is if the winds in the model will approach a state of quasi-geostrophy.

An example of quasi-geostrophic motion can be obtained by adopting a model of a homogeneous fluid which is disturbed by addition of fluid in some areas and removal of fluid in other areas in such a way that the net addition of fluid is zero. The equation of the experiment are given in (11.1).

$$\begin{aligned}
\frac{\delta u}{\delta t} + u\frac{\delta u}{\delta x} + v\frac{\delta u}{\delta y} &= -\frac{\delta \Phi}{\delta x} + fv - \varepsilon u \\
\frac{\delta v}{\delta t} + u\frac{\delta v}{\delta x} + v\frac{\delta v}{\delta y} &= -\frac{\delta \Phi}{\delta y} + fu - \varepsilon v \qquad (11.1) \\
\frac{\delta \Phi}{\delta t} + \frac{\delta(\Phi u)}{\delta x} + \frac{\delta(\Phi v)}{\delta y} &= \gamma(\Phi_F - \Phi)
\end{aligned}$$

The above equations are integrated with respect to time in a rectangular region. It is assumed that the northern and the southern boundaries behave like walls resulting in v = 0 at the wall. Periodic conditions are applied at the western and eastern boundaries. It is assumed that the grid size is 280 km. A timestep of 5 minutes is used in the integration. The dimensions are (0,31) in the x-direction and (0,17) in the y-direction. The forcing function is defined in (11.2).

$$\Phi_F = \Phi_a \sin\left(\pi \frac{j-1}{j_m-1}\right) \sin\left(2\pi \frac{i-1}{i_m-1}\right) \qquad (11.2)$$
$$\Phi_a = 2000 m^2 s^{-2}$$

At the end of a time integration the geostrophic wind components were calculated from the predicted geopotential field. The magnitudes of the model wind and the geostrophic wind were also calculated after the time integration. Figure 38 shows the comparison between the model wind and the geostrophic wind after an integra-

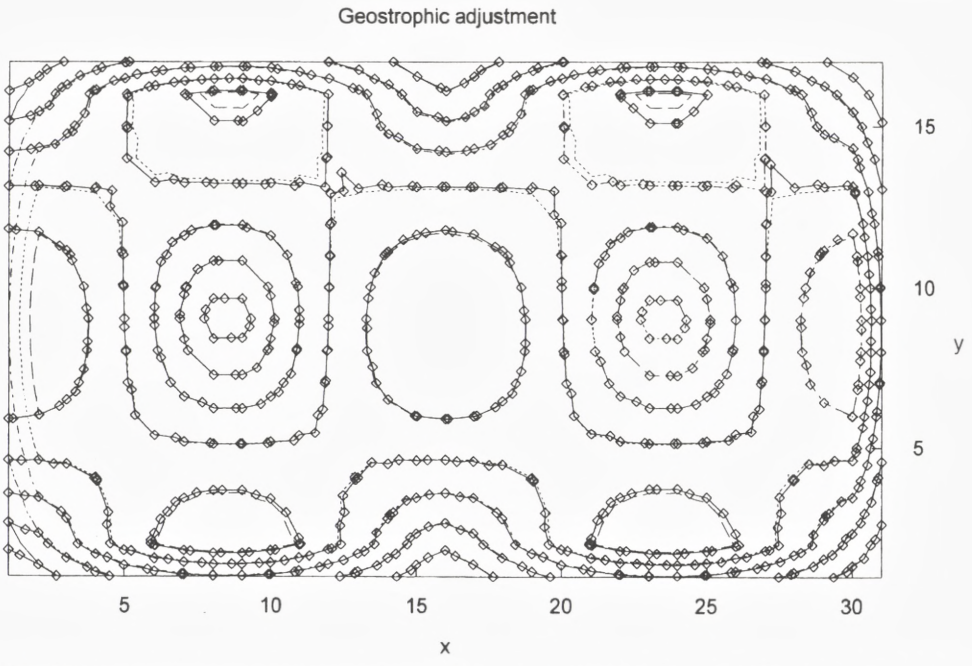


Fig. 38: A comparison between the predicted winds in the model based on the primitive equations and the calculated geostrophic winds at the same time.

tion over 51 hours. This particular time is selected because the winds at t = 51 hours are at a maximum in the central part of the region. It is seen that the model winds have become almost geostrophic during the integration.

## 12. The vertical velocity

The vertical velocity is an important parameter in meteorology, because it has a major influence on the formation and disappearence of clouds and precipitation. In addition it determines the conversion from available potential energy to kinetic energy. In spite of its importance it does not belong to the parameters which can be observed with the present procedures for local and global routine observations. Due to its importance it is a necessity to provide procedures by which the vertical velocity can be computed from the other observed quantities.

Using the pressure as the vertical coordinate it would be natural to compute the vertical p-velocity from the continuity equation as given in (12.1).

$$\frac{\delta u}{\delta x} + \frac{\delta v}{\delta y} + \frac{\delta \omega}{\delta p} = 0 \qquad (12.1)$$

Considering a vertical column the horizontal divergence can in principle be calculated from the partial derivatives of u and v. Integrating from the top where the vertical p-velocity is zero at p = 0 one can then integrate equation (12.1) and calculate the vertical p-velocity at the required levels. Such calculations have been attempted. It turns out that the values of u and v are so inaccurate that the errors in the calculation of the horizontal divergence are too large to provide an acceptable values of the vertical p-velocity.

It turns out that a better procedure is to use the fact that the observed state of the atmosphere is quasi-geostrophic. The valid equations are thus the quasi-geostrophic vorticity equation and the thermodynamic equation. These equations are given in (12.2) where we for simplicity have disregarded the heating and the dissipation. In addition, we have introduced the ordinary simplifications in the vorticity equation such as disregarding the relative vorticity as compared to the Coriolis parameter.

$$\frac{\delta \zeta}{\delta t} + u\frac{\delta \zeta}{\delta x} + v\frac{\delta \zeta}{\delta y} = f_o \frac{\delta \omega}{\delta p}$$

$$\frac{\delta}{\delta t}\left(\frac{\delta \psi}{\delta p}\right) + u\frac{\delta}{\delta x}\left(\frac{\delta \psi}{\delta p}\right) + v\frac{\delta}{\delta y}\left(\frac{\delta \psi}{\delta p}\right) + \sigma\omega = 0 \qquad (12.2)$$

$$\psi = \frac{\Phi}{f_o}\ ;\ \zeta = \frac{\delta^2 \psi}{\delta x^2} + \frac{\delta^2 \psi}{\delta y^2}$$

The time derivatives are eliminated by differentiation of the vorticity with respect to p, taking the Laplacian of the thermodynamic equation and subtracting the resulting equations. The result is the so-called omega-equation which after rearrangement is shown in (12.3).

$$f_o^2 \frac{\delta^2 \omega}{\delta p^2} + \sigma \nabla^2 \omega = G$$

$$G = f_o\left[\frac{\delta}{\delta p}\left(u\frac{\delta \zeta}{\delta x} + v\frac{\delta \zeta}{\delta y} + \beta\frac{\delta \psi}{\delta x}\right) - \nabla^2\left(u\frac{\delta}{\delta x}\left(\frac{\delta \psi}{\delta p}\right) + v\frac{\delta}{\delta y}\left(\frac{\delta \psi}{\delta p}\right)\right)\right] \qquad (12.3)$$

The right hand side of the equation in (12.3) may be calculated from fields of the geopotential. The equation may then be solved for the vertical p-velocity by numerical procedures. For the present purpose we shall be satisfied by obtaining solutions

for relatively simple specifications of the streamfunction. The static stability parameter appearing in (12.3) as a factor in front of the Laplacian may either be assumed to be a constant or increasing with decreasing values of the pressure. Calculations of the static stability parameter from observations show that the parameter is inversely proportional to the square of the pressure. When this relation is introduced in the omega-equation in (12.3) we get an equation as shown in (12.4).

$$p_*^2 \frac{\delta^2 \omega}{\delta p_*^2} + \frac{\sigma_o p_o^2}{f_o^2} \nabla^2 \omega = p_*^2 \frac{G}{f_o^2} \tag{12.4}$$

The evaluation of the function G is based on the assumption that both the basic zonal wind and the streamfunction of a wave with a single wave number increase linearly from the surface of the Earth to the tropopause, assumed to be at 250 hPa, whereafter they decrease linearly to the value 0 at the top of the atmosphere. Under these simple conditions the equation (12.4) may be solved analytically. The result is shown in Figure 39 which indicates that the vertical p-velocity has opposite signs in the stratosphere and the troposphere.

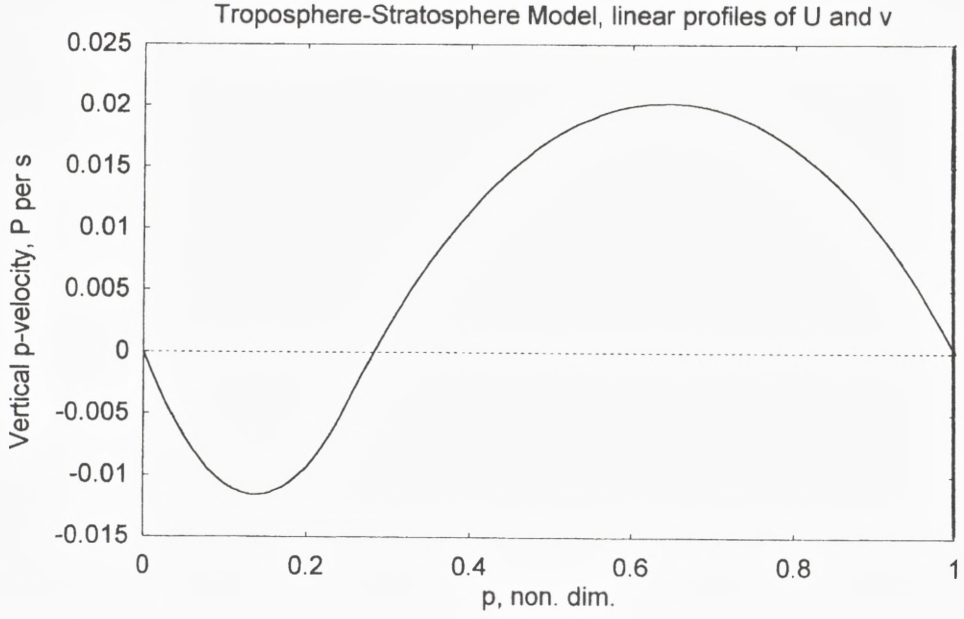


Fig. 39: The vertical p-velocity as a function of non-dimensional pressure. The zonal wind and the eddy streamfunction increases linearly from the surface to the tropopause and decrease linearly to the top of the atmosphere.

Simpler models using finite differences in the vertical direction may also be used. In the two-level model we have only one vertical velocity at 500 hPa in each vertical column. Figure 40 shows the streamfunction at 500 hPa and for the thermal flow. As is typical for the atmosphere, the thermal streamfunction (dotted curve) is located to the west of the streamfunction at 500 hPa (solid curve). The vertical p-velocity is shown in Figure 41 together with the thermal streamfunction (dotted curve). We notice the fact that the omega curve is mostly positive where the thermal streamfunction is negative. This means of course that on average the warm air is rising and the cold air is sinking. Another conclusion from this fact is that the contribution from the vertical p-velocity and the thermal streamfunction to the energy conversion from eddy available potential energy to eddy kinetic energy is positive.

We turn next to the three-level model. Figure 42 shows the three streamfunctions for the levels in the model. They are also in this case selected in such a way that the wave is tilting from east to west as the presuure is decreasing in the vertical direction. Figure 43 shows the computed vertical velocities at the pressure levels $p_o/3$ and $2\ p_o/3$. We notice again from Figure 40 and 41 the fact that on average the warm air is rising and the cold air is sinking.

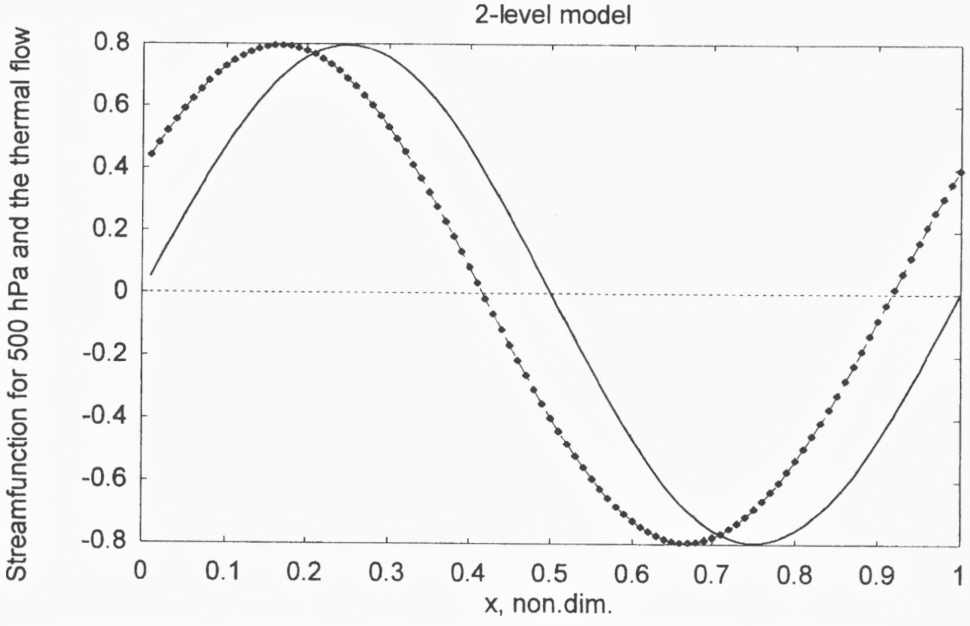


Fig. 40: The 500 hPa streamfunction (solid curve) and the thermal streamfunction (dotted cureve) in the two level model.

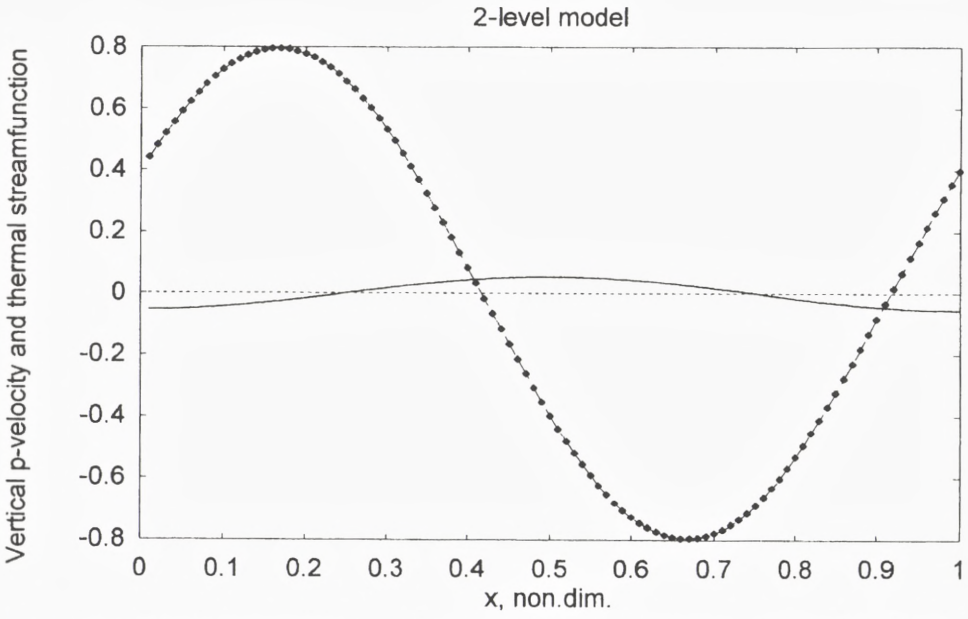


Fig. 41: The vertical p-velocity (solic curve) computed from the specification in Figure 40. The dotted curve is the thermal streamfunction.

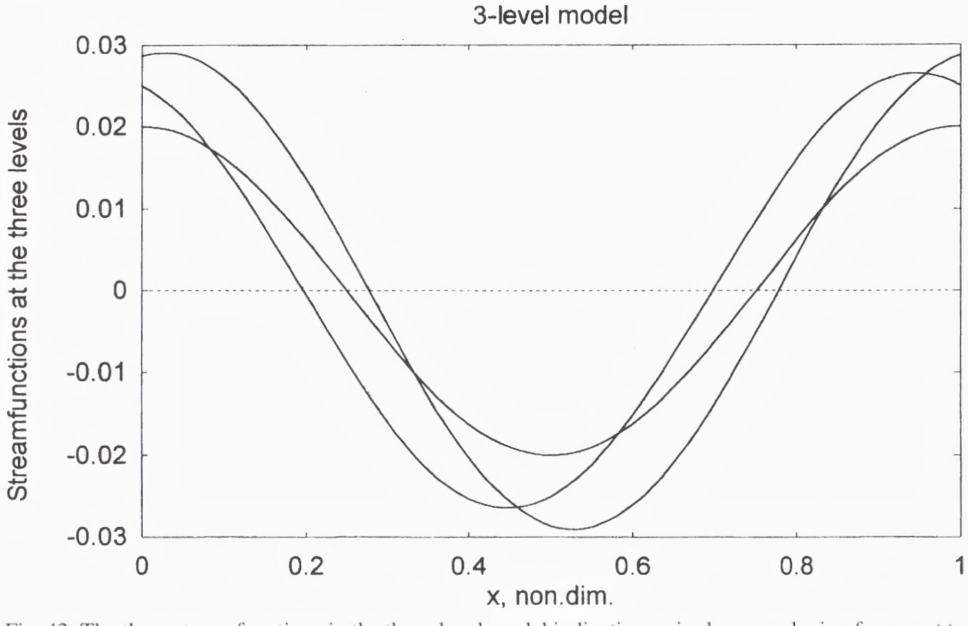


Fig. 42: The three streamfunctions in the three-level model indicating a single wave sloping from east to west as the pressure decreases.

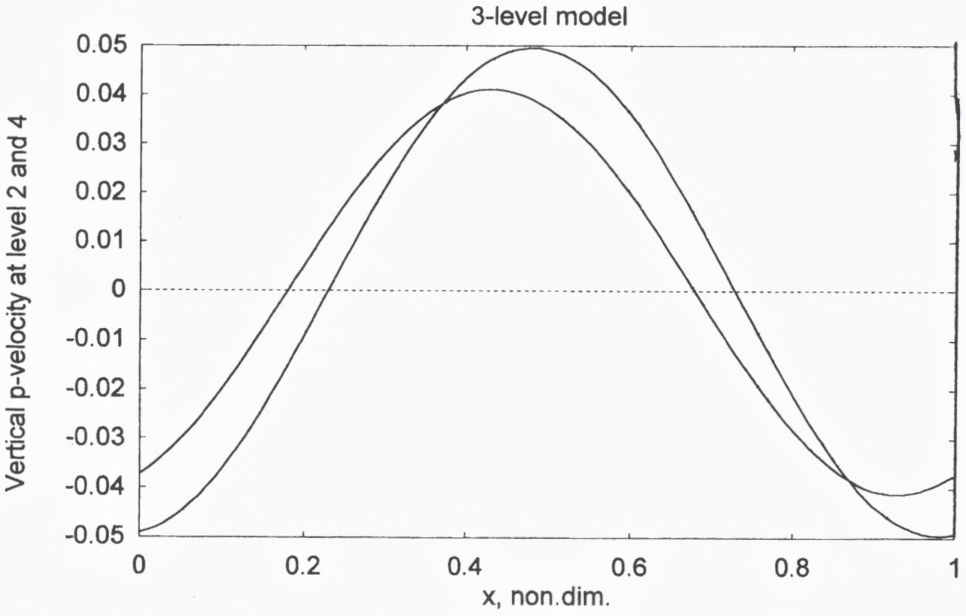


Fig. 43: The vertical p-velocities computed from the streamfunctions as shown in Figure 42.

## 13. Concluding remarks

The nature of the early work in dynamic meteorology was hampered by the nonlinearity in the equations of motion. Any closed solutions of rather general problems were impossible. The early theoretical work in dynamic meteorology was of necessity limited to problems of balance as for example the geostrophic and gradient winds as well as the vertical variations of these winds. For other problems of a theoretical nature one used mainly the perturbation technique to provide answers to many problems such as the questions of stability of atmospheric waves resulting in the investigations of the stability of baroclinic and barotropic flows.

As fast computers became available in the middle of the 20'th century with a rapid increase in both capacity and speed, it became possible to develop a series of so-called quasi-geostrophic atmospheric models ranging from the barotropic model to baroclinic models with increasing resolution in both the horizontal and the vertical directions. These models have been important for both the numerical weather predictions and for the simulation of the climate of the Earth, primarily after a quite realistic inclusion of the heating and the dissipation. The meteorological publications from the second half of the 20'th century contain a multitude of studies documenting the advances in both weather predictability and climate simulations.

The great emphasis on these studies has apparently resulted in a declining interest in theoretical studies of the nonlinear problems in dynamic meteorology. The present study is an attempt to consider the well known stability studies of atmospheric flows using not only the perturbation method, but also a numerical treatment of the nonlinear equations for an extremely simple model using only a single wavelength and a simple specification of the heating and the dissipation. In addition, several of the stability studies are based on the primitive equations and not only on quasi-nondivergent models.

The results obtained in this way are an expansion of the classical stability studies to the nonlinear domain using numerical integrations. In the most general case we use the vorticity and divergence equations coupled with the thermodynamic and the continuity equations. The treatment provides not only the growth of unstable waves, but also the development of the shape of the atmospheric waves through the exchanges of energy between the zonal state and the eddies including the asymptotic approach to a steady state. The general model develops waves with both momentum and sensible heat transports by the waves and an energetics which is similar to the observed diagrams with respect to directions and in reasonable agreement with the magnitudes recalling that the model contains one wavelength only. The only major difference between the model and the atmosphere is the relatively large negative velocity of the very long waves.

The paper contains also an analysis of the three-level quasi-nondivergent model in order to show that also this model with vertical variation of the static stability is unstable for the very long waves. Some general cases of two- and three-dimensional trajectories for inertial motion are included in the study. In Section 8 the thermal wave speeds for a tropospheric continuous model are determined under the conditions that the vertical p- velocity vanishes at the pressure levels $p = p_T$ and $p = p_o$, where $p_T$ is larger than zero.

Numerical experiments with an atmospheric model indicate the time it takes for the model, starting from rest, to reach a quasi-geostrophic state. It happens in 2 to 3 days.

In the investigations of the various wave types it has been emphasized that very large values of the phase speed are present for the thermal waves and for the long waves from both the inertial and the Rossby waves. At the end of the paper we should mention that these large wave speeds create no serious problems when care is taken to start from a state in quasi-geostrophic balance, see Machenhauer (1977) and Kuo (1997).

# References

Charney, J. G., 1947: The dynamics of long waves in a baroclinic westerly current, Jour. of Meteor., *4*, 135-162.

Charney, J. G. and A. Eliassen, 1949: A numerical method for predicting the perturbations on the middle-latitude westerlies, Tellus, *1*, 38-54.

Charney, J. G., R. Fjørtoft and J. von Neumann, 1950: Numerical integration of the barotropic vorticity equation, Tellus, *2*, 237-254.

Cressman, G.P., 1958: Barotropic divergence and very long atmospheric waves, Mo. Wea. Rev., *86*, 293-297.

Gates, W.L., 1961: The stability properties and energy transformation of the two-layer model of variable static stability, Tellus, *13*, 460-472.

Kuo, H.L., 1997: A new perspective of geostrophic adjustment, Dynamics of Atmospheres and Oceans, *27*, 413-437.

Machenhauer, B., 1977: On the dynamics of gravity oscillations in a shallow water model with applications to normal mode initialization, Beiträge zur Physik der Atmosphäre, *50*, 263-271.

Marcussen, P. and A. Wiin-Nielsen, 1999: A numerical investigation of a simple spectral model, Atmósfera, *12*, 43-73.

Phillips, N.A., 1956: The general circulation of the atmosphere: a numerical experiment, Q.J. of the Roy. Met. Soc., *82*, 123-164.

Smagorinsky, J., 1953: The dynamical influence of large-scale sources and sinks on the quasi-stationary mean motions of the atmosphere, Quart. J. Royal Meteor. Soc., *79*, 342-366.

Smagorinsky, J., 1963: General circulation experiments with the primitive equations, I. The basic experiment, Mo. Wea. Rev., *91*, 99-164.

Wiin-Nielsen, A., 1959: On barotropic and baroclinic models with special emphasis on ultra-long waves, Mo. Wea. Rev., *87*, 171-183.

Wiin-Nielsen, A. 1962: On baroclinic instability in filtered and non-filtered numerical prediction models, Tellus, *15*, 1-19.

Wiin-Nielsen, A., 1967: On the annual variation and spectral distribution of atmospheric energy, Tellus, *19*, 540-559.

Wiin-Nielsen, A., 1989: A stability investigation of a three-level, quasi-geostrophic model, Geophysica, *25*, 21-35.

Wiin-Nielsen, A., 1991: A study of global mean temperatures applied to available potential energy, annual variations and static stability, Tellus, *43A*, 15-24.

Wiin-Nielsen A., 1999: On the spectral distribution of kinetic energy in large-scale atmospheric flow, Nonlinear Processes in Geophysics, *5*, 187-192.

Wiin-Nielsen, A., 2000: A note on the logarithmic -3 law of atmospheric energy, Atmósfera, *13*, 167-176.

Wiin-Nielsen, A. and C.-T. Chen, 1993: Fundamentals of Atmospheric Energetics, Oxford University Press, 376 pp.